Electronic Supplementary Information

Modulation of argentophilic interaction by bridging amine ligand: tuneable photoluminescence by excitation energy or temperature

Ji Zheng, Ya-Dong Yu, Fang-Fang Liu, Bao-Yu Liu, Gang Wei and Xiao-Chun Huang*
Department of Chemistry, Shantou University, Guangdong, 515063, P. R. China.
E-mail: xchuang@stu.edu.cn

Contents

Experimental Section.....**S3**
Materials and physical measurements.....**S3**
Synthesis of the complexes.....**S3**
Crystal Data Section.....**S4**
Table S1 Data summary.....**S5**
Table S2 Bond lengths and angles.....**S6**
Structural Description Section.....**S9**
The analysis of coordination environment around Ag atoms.....**S9**
Fig. S1 The coordination environments around Ag atoms.....**S9**
Table S3 The comparison of geometry and the MBO.....**S10**
*Table S4 The selected bond lengths, bond angles and MBO of complex **2-4***.....**S10**
The supramolecular interactions and packing patterns.....**S12**
*Table S5 Supramolecular interactions of **1** and **2***.....**S12**
*Fig. S2 Supramolecular interactions of (a) **1** and (b) **2***.....**S12**
*Fig. S3 The packing view of **1** (a) and **2** (b)*.....**S12**
*Fig. S4 The 1D chain of **3** (a) and **4** (b)*.....**S13**
*Table S6 Hydrogen bonds of **3** and **4***.....**S13**
*Fig. S5 The packing view of **3** (a) and **4** (b) through hydrogen bonds*.....**S14**
Physical Measurement Section.....**S15**
Fig. S6 PXRD patterns.....**S15**
Fig. S7 The room-temperature solid state UV-Vis absorption spectra.....**S16**
Fig. S8 The photographs of crystals.....**S16**
*Fig. S9 The temperature-dependant solid state photoluminescent spectra of **1***.....**S17**
*Fig. S10 The temperature-dependant solid state photoluminescent spectra of **2***.....**S17**
*Fig. S11 The temperature-dependant solid state photoluminescent spectra of **3***.....**S18**
*Fig. S12 The temperature-dependant solid state photoluminescent spectra of **4***.....**S18**
*Fig. S13 Selected luminescence decay of **1***.....***S19***
*Fig. S14 Selected luminescence decay of **2***.....***S19***
*Fig. S15 Selected luminescence decay of **3***.....***S20***
*Fig. S16 Selected luminescence decay of **4***.....***S20***
*Table S7 The emission life times (τ) of **1-4***.....**S21**
*Fig. S17 The luminescent spectra of **1** before and after grinding*.....**S21**

Fig. S18 CIE for ***1-4*** **S22**
Fig. S19 The room temperature solid state photoluminescent spectrum of ***1*** **S22**
DFT Calculation Section **S22**
Computation details **S22**
The assignment analysis of LE absorptions for complex ***1-4*** **S23**
Fig. S20 The simulated UV-Vis absorption spectra **S25**
Table S8 First 50 lowest energy singlet-singlet excitation for complex ***1*** *by TD-DFT* **S25**
Table S9 First 50 lowest energy singlet-singlet excitation for complex ***2*** *by TD-DFT* **S26**
Table S10 First 50 lowest energy singlet-singlet excitation for complex ***3*** *by TD-DFT* **S28**
Table S11 First 50 lowest energy singlet-singlet excitation for complex ***4*** *by TD-DFT* **S30**
Fig. S21 Selected molecular orbitals for complex ***1*** **S32**
Fig. S22 Selected molecular orbitals for complex ***2*** **S32**
Fig. S23 Selected molecular orbitals for complex ***3*** **S33**
Fig. S24 Selected molecular orbitals for complex ***4*** **S33**
Table S12 Orbital compositions of selected molecular orbitals for ***1*** **S34**
Table S13 Orbital compositions of selected molecular orbitals for ***2*** **S34**
Table S14 Orbital compositions of selected molecular orbitals for ***3*** **S34**
Table S15 Orbital compositions of selected molecular orbitals for ***4*** **S34**
Table S16 Orbital energy of HOMO, LUMO, and HOMO-LUMO gaps **S35**
Fig. S25 SOMOs for the T_1 *state of complex* ***1*** **S35**
Table S17 Orbital energy levels of SOMOs of T_1 *state for* ***1*** **S35**
Table S18 The orbital compositions of ***1*** *based on different models* **S35**
Table S19 The orbital compositions of ***2*** *based on different models* **S36**
Table S20 The orbital compositions of S_0 *states of* ***3*** *and* ***4*** **S36**
Table S21 The orbital compositions of T_1 *states of* ***3*** *and* ***4*** **S36**
References **S36**

Experimental Section

Materials and Physical Measurements

All the commercially available reagents were used as received without further purification. Microwave-assisted solvothermal syntheses were carried out in a microwave oven (Initiator 8 EXP, 2450 MHz frequency, Biotage Corp). UV-Vis absorption spectra were collected by Lambda 950 UV/Vis spectrometer (KBr pellets). Photoluminescent properties were determined by a Edinburgh Analytical instrument FLS920. Infrared spectra were recorded on a Nicolet Avatar 360 FTIR spectrometer in the range of 4000-400cm^{-1} (KBr pellets). The phase purity of each complex was checked by powder X-ray diffraction (PXRD) with Cu Kα radiation (1.5418 Å) on a Rigaku D/M-2200T automated diffractometer.

Synthesis of the complexes:

$[Ag_2(Hpidc)(NH_3)_2]$ (**1**): A mixture of $AgNO_3$ (0.2 mmol, 0.0340 g), H_3pidc (0.1 mmol, 0.0233 g), MeCN (6.0 mL) and aqueous ammonia (25%, 1.0 mL) was sealed in a 15-mL Teflon-lined stainless autoclave, heated at 120 °C for three days, and then slowly cooled to room temperature at a rate of 6 ℃/h. Pale yellow block crystals of **1** were obtained in *ca.* 85% yield based on H_3pidc. Elemental analysis calcd (%) for $C_{10}H_{11}Ag_2N_5O_4$: C 24.97, H 2.31,N 14.56; found: C 24.87, H 2.26,N 14.63; IR (KBr): IR (KBr pellet, cm^{-1}): 3319(m)，3170(m)，1557(s)，1598(s)，1478(s)，1416(s)，1366(s)，1262(m)，1200(s)，1146(m)，1117(m)，1001(m)，865(m)，798(w)，628(w)。

$[Ag_2(Hpidc)(NH_3)_2]_2{\cdot}2H_2O$ (**2**): A solution of $AgNO_3$ (1.0 mmol, 0.170 g) in MeCN (5.0 mL) was added to a solution of H_3pidc (0.05 mmol, 0.117 g) in aqueous ammonia (25%, 10 mL). The resulting clear solution was left standing in the dark for several hours to give colorless needle crystals in *ca.* 85% yield based on H_3pidc. Elemental analysis calcd (%) for $C_{20}H_{26}Ag_4N_{14}O_{10}$: C 24.07, H 2.63, N 19.65; found: C 24.03, H 2.67, N 19.61 IR (KBr): IR (KBr pellet, cm^{-1}): 3319(m)，3170(m)，1557(s)，1598(s)，1478(s)，1416(s)，1366(s)，1262(m)，1200(s)，1146(m)，1117(m)，1001(m)，865(m)，798(w)，628(w)

$[Ag_2(Hpidc)(en)]_2$ (**3**): A mixture of $AgNO_3$ (0.3 mmol, 0.0510 g), H_3pidc (0.1 mmol, 0.0233 g), MeCN (24.0 mL) and 0.5 mL of 1,2-ethylenediamine anhydrous was sealed in a 60-mL Teflon-lined autoclave. The mixture was heated at 120 °C by microwave under autogenous pressure for 140 min, and then cooled to room temperature. Colorless columnar crystals of **3** were

obtained in *ca.* 45% yield based on H_3pidc. Elemental analysis calcd (%) for $C_{12}H_{13}Ag_2N_5O_4$: C 28.43, H 2.58, N 13.81; found: C 28.41, H 2.54, N 13.84; IR (KBr pellet, cm^{-1}): 3319(m)，3170(m)，1631(s)，1590(s)，1507(s)，1411(s)，1362(s)，1262(m)，1150(s)，1117(m)，997(m)，843(m)，794(m)，706(w)，623(w)。

$[Ag_4(Hpidc)_2(pn)_2]$ (**4**): A mixture of $AgNO_3$ (0.1 mmol, 0.0170 g), H_3pidc (0.5 mmol, 0.0117 g), MeCN (3.0 mL), H_2O(3.0 mL) and 1,3-propanediamine (98%, 5 drops) was sealed in a 15mL Teflon-lined stainless autoclave and heated at 100 °C for 24 h, and then slowly cooled to room temperature at a rate of 2 ℃/h. Yellow block crystals of **4** were obtained in *ca.* 55% yield based on H_3pidc. Elemental analysis calcd (%) for $C_{26}H_{30}Ag_4N_{10}O_8$: C 29.97, H2.90, N 13.44; found: C 29.94, H2.92, N 13.46; IR (KBr): IR (KBr pellet, cm^{-1}): 3319(m)，3141(m)，1631(s)，1577(s)，1503(s)，1461(s)，1366(s)，1258(m)，1117(s)，1001(m)，847(m)，789(m)，740(m)，702(w)，619(w)。

Crystal Data Section

All single crystals of these four complexes were carefully selected under an optical microscope and glued to thin glass fibers. Structural measurements were performed on a computer-controlled Siemens Smart CCD diffractometer with graphite-monochromated Mo Kα radiation (λ = 0.71073 Å). Absorption corrections were applied by using the multiscan program SADABS. Structural solutions and full-matrix least-square refinements based on F^2 were performed with the SHELX-97 program packages, respectively. Anisotropic thermal parameters were applied to all non-hydrogen atoms. All the hydrogen atoms were generated geometrically. Crystal data as well as details of data collection and refinements for the complexes are summarized in Table S1. Selected structural characteristics are given in Table S2.

Table S1 Crystallographic data and structure refinement of **1** - **4**.

	1 (298k)	**1** (100k)	**2** (298k)
Empirical formula	$C_{10}H_{11}Ag_2N_5O_4$	$C_{10}H_{11}Ag_2N_5O_4$	$C_{20}H_{26}Ag_4N_{14}O_{10}$
Formula weight	480.98	480.98	997.99
Crystal system	Monoclinic	Monoclinic	Monoclinic
Space group	$P2_1/n$	$P2_1/n$	$P2_1/n$
a (Å)	10.4687(8)	10.4635(4)	6.8790(8)
b (Å)	12.6970(10)	12.5188(3)	11.7678(14)
c (Å)	11.0554(8)	11.0115(4)	17.321(2)
β (deg)	115.1220(10)	115.202(4)	92.741(2)
V (Å^3)	1330.491(17)	1305.10(8)	1400.5(3)
Z	4	4	2
Temperature (K)	298(2)	100(2)	298(2)
D_{calcd} (g·cm^{-3})	2.401	2.448	2.367
R_{int}	0.0224	0.0227	0.0280
GOF	1.107	1.089	1.003
R_1[a] [I > 2σ(I)]	0.0327	0.0326	0.0306
wR_2[b] (all data)	0.0843	0.1312	0.0958
ρ_{fin} (max/min) (eÅ^{-3})	0.859/-0.505	1.724/-0.895	0.497/-0.641
	2 (100k)	**3**	**4**
Empirical formula	$C_{20}H_{26}Ag_4N_{14}O_{10}$	$C_{24}H_{26}Ag_4N_{10}O_8$	$C_{26}H_{30}Ag_4N_{10}O_8$
Formula weight	997.99	1014.03	1042.08
Crystal system	Monoclinic	Monoclinic	Monoclinic
Space group	$P2_1/n$	$P2_1/c$	$P2_1/c$
a (Å)	6.7585(2)	8.9949(4)	14.2975(6)
b (Å)	11.7522(5)	14.1156(6)	11.9979(6)
c (Å)	17.2702(6)	11.5353(6)	19.3757(7)
β (deg)	92.669(3)	104.168(5)	109.377(4)
V (Å^3)	1370.24(9)	1420.07(11)	3135.4(2)

Z	2	2	4
Temperature (K)	100(2)	298(2)	298(2)
D_{calcd} (g·cm^{-3})	2.419	2.371	2.208
R_{int}	0.0350	0.0413	0.0375
GOF	1.003	1.018	0.999
R_1[a] [I > 2σ(I)]	0.0288	0.0398	0.0754
wR_2[b] (all data)	0.0651	0.0939	0.2342
ρ_{fin}(max/min)(eÅ^{-3})	0.646/-0.864	0.600/-0.713	3.572/-2.295

[a] $R_1 = \sum|F_o| - |F_c||/\sum|F_o|$; [b] $wR_2 = \{[\sum w(F_o^2-F_c^2)^2]/\sum[w(Fo^2)^2]\}^{1/2}$;

$w = 1/ [\sigma^2(F_o^2) + (aP)^2 + bP]$, where $P= [\max(F_o^2, 0) + 2F_c^2]/3$ for all data.

Table S2 Selected bond lengths (Å) and bond angles (°) of **1**~**4**.

Complex 1 (298k)			
Ag(1)-Ag(2)#1	3. 571(6)	Ag(1)-N(5)	2.128(4)
Ag(1)-N(2)	2.137(3)	Ag(1)-N(1)	2.663(4)
Ag(1)-O(3)	3.009(3)	Ag(2)-N(4)	2.136(4)
Ag(2)-N(3)	2.163(3)	Ag(2)-O(1)	2.593(3)
N(5)-Ag(1)-N(2)	167.87(14)	N(1)-Ag(1)-O(3)	131.94(10)
N(5)-Ag(1)-N(1)	120.96(13)	N(4)-Ag(2)-N(3)	168.98(14)
N(2)-Ag(1)-N(1)	69.00(12)	N(4)-Ag(2)-O(1)	116.22(14)
N(5)-Ag(1)-O(3)	107.10(12)	N(3)-Ag(2)-O(1)	71.24(11)
N(2)-Ag(1)-O(3)	63.31(11)		
Complex 1 (100k)			
Ag(1)-Ag(2)#1	3.515(6)	Ag(1)-N(5)	2.131(5)
Ag(1)-N(2)	2.140(4)	Ag(1)-N(1)	2.679(5)
Ag(1)-O(3)	2.977(3)	Ag(2)-N(4)	2.136(5)
Ag(2)-N(3)	2.152(4)	Ag(2)-O(1)	2.601(4)
N(5)-Ag(1)-N(2)	168.19(17)	N(1)-Ag(1)-O(3)	132.31(13)
N(5)-Ag(1)-N(1)	120.16(16)	N(4)-Ag(2)-N(3)	169.24(17)
N(2)-Ag(1)-N(1)	68.95(16)	N(4)-Ag(2)-O(1)	115.26(15)

N(5)-Ag(1)-O(3)	107.54(14)	N(3)-Ag(2)-O(1)	71.26(13)
N(2)-Ag(1)-O(3)	63.83(14)		

Complex 2 (298k)

Ag(1)-Ag(2)#1	3.054(6)	Ag(1)-N(3)	2.147(4)
Ag(1)-N(4)	2.158(4)	Ag(1)-O(4)	2.675(4)
Ag(2)-N(5)	2.141(4)	Ag(2)-N(2)	2.164(4)
Ag(2)-N(1)	2.485(4)	Ag(2)-O(1)	3.145(4)
N(3)-Ag(1)-N(4)	172.72(15)	N(2)-Ag(2)-N(1)	71.88(13)
N(3)-Ag(1)-O(4)	69.71(12)	N(5)-Ag(2)-O(1)	106.16(14)
N(4)-Ag(1)-O(4)	117.43(14)	N(2)-Ag(2)-O(1)	60.20(11)
N(5)-Ag(2)-N(2)	163.33(16)	N(1)-Ag(2)-O(1)	131.68(11)
N(5)-Ag(2)-N(1)	122.13(15)		

Complex 2 (100k)

Ag(1)-Ag(2)#1	3.0131(5)	Ag(1)-N(3)	2.133(4)
Ag(1)-N(4)	2.143(4)	Ag(1)-O(4)	2.687(3)
Ag(2)-N(5)	2.142(4)	Ag(2)-N(2)	2.165(4)
Ag(2)-N(1)	2.476(4)	Ag(2)-O(1)	3.143(3)
N(3)-Ag(1)-N(4)	173.30(14)	N(2)-Ag(2)-N(1)	71.94(13)
N(3)-Ag(1)-O(4)	69.81(12)	N(5)-Ag(2)-O(1)	105.48(13)
N(4)-Ag(1)-O(4)	116.72(13)	N(2)-Ag(2)-O(1)	60.32(11)
N(5)-Ag(2)-N(2)	162.71(15)	N(1)-Ag(2)-O(1)	131.82(11)
N(5)-Ag(2)-N(1)	122.67(14)		

Complex 3

Ag(1)-Ag(2)#1	2.947(7)	Ag(1)-Ag(1)#2	3.191(9)
Ag(1)-N(2)	2.211(4)	Ag(2)-N(3)	2.176(4)
Ag(1)-N(5)#1	2.207(4)	Ag(2)-N(4)	2.169(4)
Ag(1)-N(1)	2.555(5)	Ag(2)-O(3)	2.593(4)
Ag(1)-O(2)	3.229(4)		
N(2)-Ag(1)-N(5)#1	158.96(17)	N(1)-Ag(1)-O(2)	129.67(13)

N(2)-Ag(1)-N(1)	70.69(15)	N(3)-Ag(2)-N(4)	166.74(18)
N(5)#1-Ag(1)-N(1)	119.17(16)	N(3)-Ag(2)-O(3)	71.51(15)
N(2)-Ag(1)-O(2)	59.05(13)	N(4)-Ag(2)-O(3)	115.55(16)
N(5)#1-Ag(1)-O(2)	109.30(15)		

Complex 4

Ag(1)-Ag(4)	4.172(2)	Ag(2)-Ag(3)	3.8403(18)
Ag(3)-Ag(4)#1	3.2362(18)	Ag(1)-N(5)	2.122(8)
Ag(1)-N(10)	2.141(13)	Ag(1)-O(1)	2.589(9)
Ag(2)-N(2)	2.135(8)	Ag(2)-N(8)	2.145(10)
Ag(2)-O(7)	2.601(9)	Ag(3)-N(4)	2.133(9)
Ag(3)-N(7)	2.132(12)	Ag(3)-N(6)	2.814(11)
Ag(3)-O(4)	2.888(10)	Ag(4)-N(1)	2.142(9)
Ag(4)-N(9)	2.149(9)	Ag(4)-O(8)	2.813(11)
Ag(4)-N(3)	2.873(12)		
N(5)-Ag(1)-N(10)	169.5(4)	N(4)-Ag(3)-O(4)	65.7(3)
N(5)-Ag(1)-O(1)	71.8(3)	N(7)-Ag(3)-O(4)	105.2(4)
N(10)-Ag(1)-O(1)	111.7(4)	N(6)-Ag(3)-O(4)	129.3(3)
N(2)-Ag(2)-N(8)	173.4(4)	N(1)-Ag(4)-N(9)	173.4(4)
N(2)-Ag(2)-O(7)	71.3(3)	N(1)-Ag(4)-O(8)	66.6(3)
N(8)-Ag(2)-O(7)	113.7(4)	N(9)-Ag(4)-O(8)	110.8(3)
N(4)-Ag(3)-N(7)	170.8(4)	N(1)-Ag(4)-N(3)	65.4(3)
N(4)-Ag(3)-N(6)	65.5(3)	N(9)-Ag(4)-N(3)	117.8(4)
N(7)-Ag(3)-N(6)	122.9(4)	O(8)-Ag(4)-N(3)	131.3(3)

Symmetry code: #1 -x,-y,-z+1 (**1**); #1 -x,-y,-z (**2**); #1 -x,-y,-z+1
#2 -x+1,-y,-z+1(**3**); #1 x,-y+3/2, z+1/2 (**4**).

Structural Description Section

The analysis of coordination environment around Ag atoms

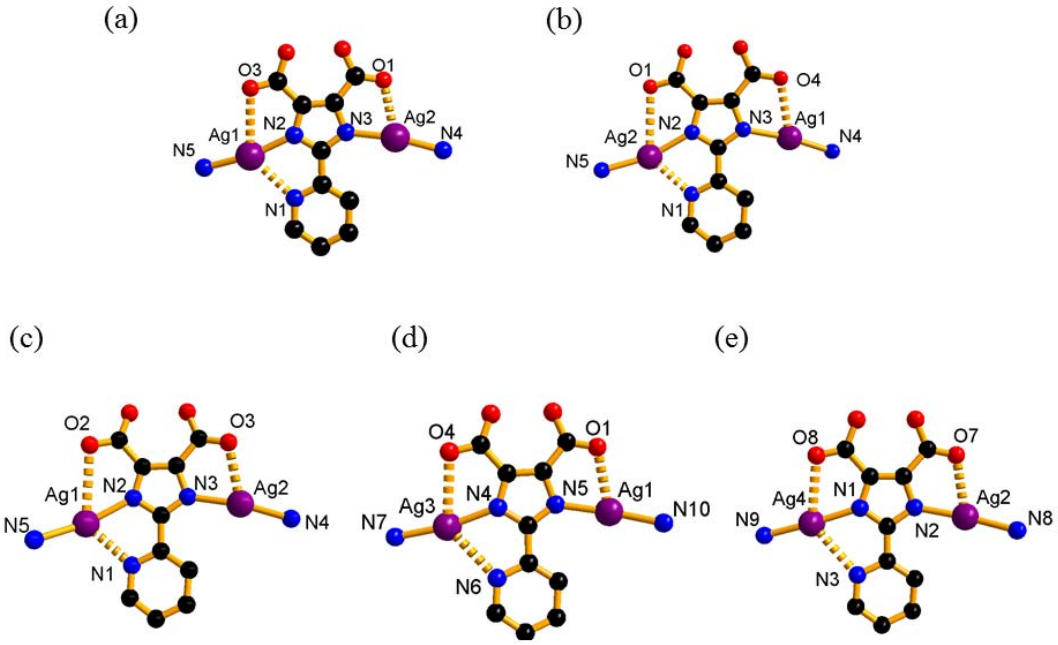

Fig. S1 The coordination environments around silver atoms in (a) **1,** (b) **2,** (c) **3** and (d) (e) **4.**

By analyzing the X-ray diffraction data of the complex **1**, both the N_{am}-Ag-N_{im} angles of Ag1 and Ag2 are near 180°, and the bond length of Ag-N_{py} is significantly longer than the Ag-N_{im} and Ag-N_{am}, suggesting that the coordinate geometry of Ag atoms should be linear two-coordinate (The N atom from imidazolyl and pyridinyl of $Hpidc^{2-}$ are denoted as N_{im} and N_{py}, respectively. The N atom from auxiliary amine ligand is denoted as N_{am}. The O atom from carboxyl of $Hpidc^{2-}$ is denoted as O_{COO}^{-}.).

After optimization (Table S3), the N_{am}-Ag-N_{im} angles are still nearly 180° and the Ag-N_{im} and Ag-N_{am} are much shorter than the Ag-N_{py}. Also, the Mayer Bond Order (MBO) of Ag-N_{im} and Ag-N_{am} are significantly larger than those of Ag-N_{py} as well as of Ag-O_{COO}^{-}. Overall, the Ag atoms of complex **1** are mainly linear two-coordinate but perturbed by N_{py} or O_{COO}^{-} atom (See DFT Calculation Section for computational details).

The coordination environments around Ag atoms of complex **2-4** are also analyzed according to

the crystal structures and the MBO calculated based on their crystal structures, respectively (Table S4-S6). Similar to **1**, all the N_{am}-Ag-N_{im} angles are near 180°, especially for **4**. What's more, the bond lengths of Ag-N_{im} and Ag-N_{am} are shorter than that of Ag-N_{py} and the MBO of Ag-N_{im} and Ag-N_{am} are significantly larger than that of Ag-N_{py} of as well as of Ag-O_{COO}^-.

In summary of this part, all the Ag atoms in complex **1-4** are mainly linear two-coordinate but perturbed by N_{py} or O_{COO-} atom.

Table S3 The comparison of geometry (bond length in Å and bond angle in °) of complex **1** before and after optimization and the MBO based on the optimized geometry.

	Crystal Structure	Optimized Geometry	MBO
Ag1-N1	2.663(4)	2.923	0.1354
Ag1-N2	2.137(3)	2.144	0.4154
Ag1-N5	2.128(4)	2.213	0.4011
Ag1-O3	3.009(3)	2.636	0.2023
Ag2-N3	2.163(3)	2.170	0.4456
Ag2-N4	2.136(4)	2.215	0.4053
Ag2-O1	2.593(3)	2.368	0.3255
N5-Ag1-N2	167.87(14)	165.08	None
N4-Ag2-N3	168.98(14)	176.40	None

Table S4 The selected bond length (in Å), bond angle (in °) and MBO of complex **2-4.**

Complex **2**		
	Structural parameter	MBO
Ag(1)-Ag(2)#1	3.054(6)	0.1065
Ag2-N1	2.485(4)	0.2494
Ag2-N2	2.164(4)	0.3772
Ag2-N5	2.141(4)	0.3940
Ag2-O1	3.145(4)	0.1073
Ag1-N3	2.147(4)	0.4357
Ag1-N4	2.158(4)	0.4063
Ag1-O4	2.675(4)	0.2976
N5-Ag2-N2	163.33(16)	None
N3-Ag1-N4	172.72(15)	None
Complex **3**		
	Structural parameter	MBO
Ag(2)-Ag(1)#1	2.947(7)	0.1028
Ag1-N1	2.555(5)	0.2475
Ag1-N2	2.211(4)	0.4009
Ag1-N5	2.207(4)	0.3933
Ag1-O2	3.229(4)	0.0831

Ag2-N3	2.176(4)	0.4157
Ag2-N4	2.169(4)	0.3990
Ag2-O3	2.593(4)	0.2836
N2-Ag1-N5	158.96(17)	None
N3-Ag2-N4	166.74(18)	None
Complex **4**		
	Structural parameter	MBO
Ag1-Ag4	4.172(2)	None
Ag2-Ag3	3.8403(18)	None
Ag3-N6	2.814(11)	0.1501
Ag3-N4	2.133(9)	0.3998
Ag3-N7	2.132(12)	0.3888
Ag3-O4	2.888(10)	0.1759
Ag1-N5	2.122(8)	0.4535
Ag1-N10	2.141(13)	0.4163
Ag1-O1	2.589(9)	0.3184
N4-Ag3-N7	170.8(4)	None
N5-Ag1-N10	169.5(4)	None
Ag4-N3	2.873(12)	0.1553
Ag4-N1	2.142(9)	0.4177
Ag4-N9	2.149(9)	0.4140
Ag4-O8	2.813(11)	0.1840
Ag2-N2	2.135(8)	0.4497
Ag2-N8	2.145(10)	0.4306
Ag2-O7	2.601(9)	0.2730
N1-Ag4-N9	173.4(4)	None
N2-Ag2-N8	173.4(4)	None

Symmetry code: #1 -x,-y,-z (**2**); #1 -x,-y,-z+1 #2 -x+1,-y,-z+1(**3**).

The supramolecular interactions and packing patterns

Table S5 Supramolecular interactions of **1**and **2.**

	Intratetraunit Interactions (Å) (298k/100k)			Intertetraunit Interactions (Å) (298 K)	
	Ag-Ag	π-π	Ag-π	Hydrogen Bond	π-π
1	3.571/3.515	3.582/3.500	3.161/3.140	3.005-3.147	None
2	3.054/3.013	3.667/3.601	3.654/3.586	2.793-3.408	3.851

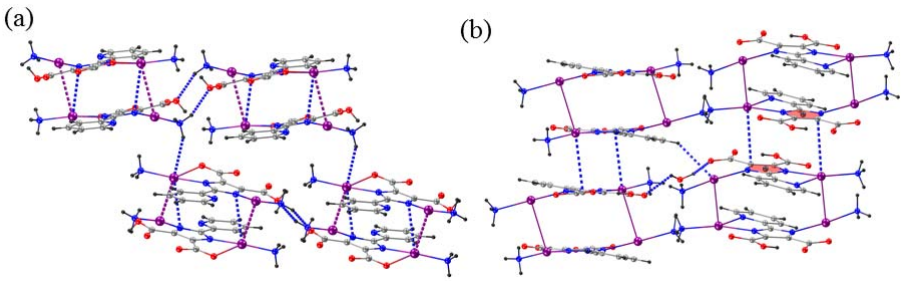

Fig. S2 Supramolecular interactions of (a) **1** and (b) **2.**

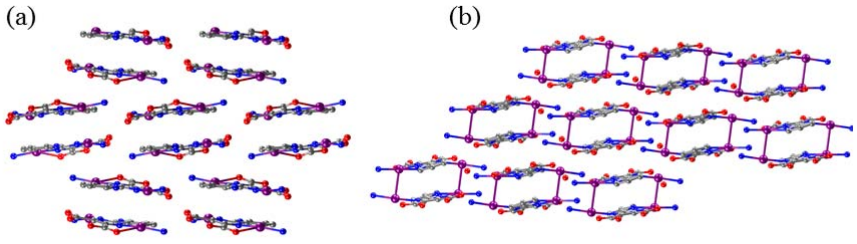

Fig. S3 The packing view of **1** (a) and **2** (b).

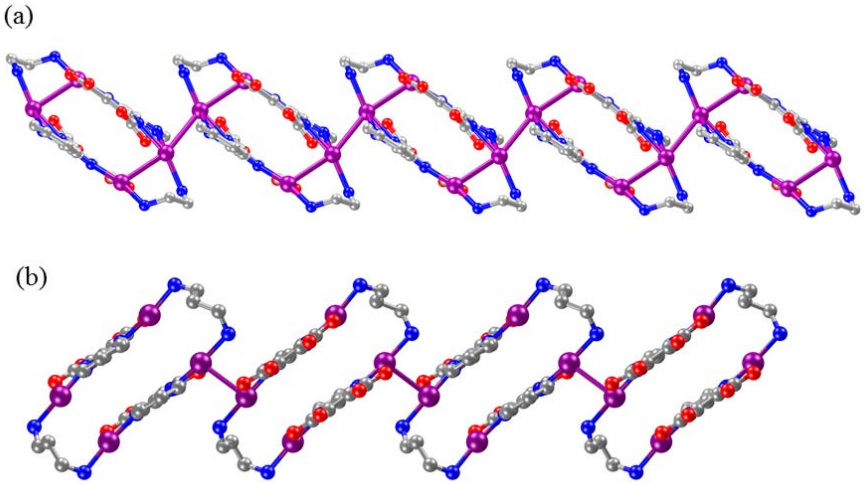

Fig. S4 The 1D chain of **3** (a) and **4** (b).

Table S6 Hydrogen bonds of **3** and **4.**

	Hydrogen bond	Bond Length (Å)	Bond Angle (°)
3	N4-H4B···O1#1	3.195	170.83
	N5-H5A···O2#1	3.113	140.21
	N4-H4C···O3#2	3.023	148.58
	N4-H4C···O4#2	3.229	126.33
4	N7-H7B···N1 #1	3.412	169.83
	N7-H7B···N3 #1	3.139	117.31
	N7-H7C···O7 #2	2.911	162.39
	N8-H8B···O4 #2	2.987	171.46
	N8-H8C···O6 #3	3.029	147.52
	N9-H9B···N4 #4	3.305	166.18
	N9-H9C···O1 #5	2.976	165.37
	N10-H10A···O8 #5	2.934	164.98
	N10-H10B···O3 #6	3.067	153.84

Symmetry code: #1 -x,y-1/2,-z+3/2 #2 x,-y-1/2,z-1/2 (**3**); #1 x,-y+3/2,z-1/2 #2 -x,-y+1,-z #3 -x,y+1/2,-z+1/2 #4 x,-y+3/2,z+1/2 #5 -x+1,-y+1,-z+1 #6 -x+1,y+1/2,-z+1/2(**4**).

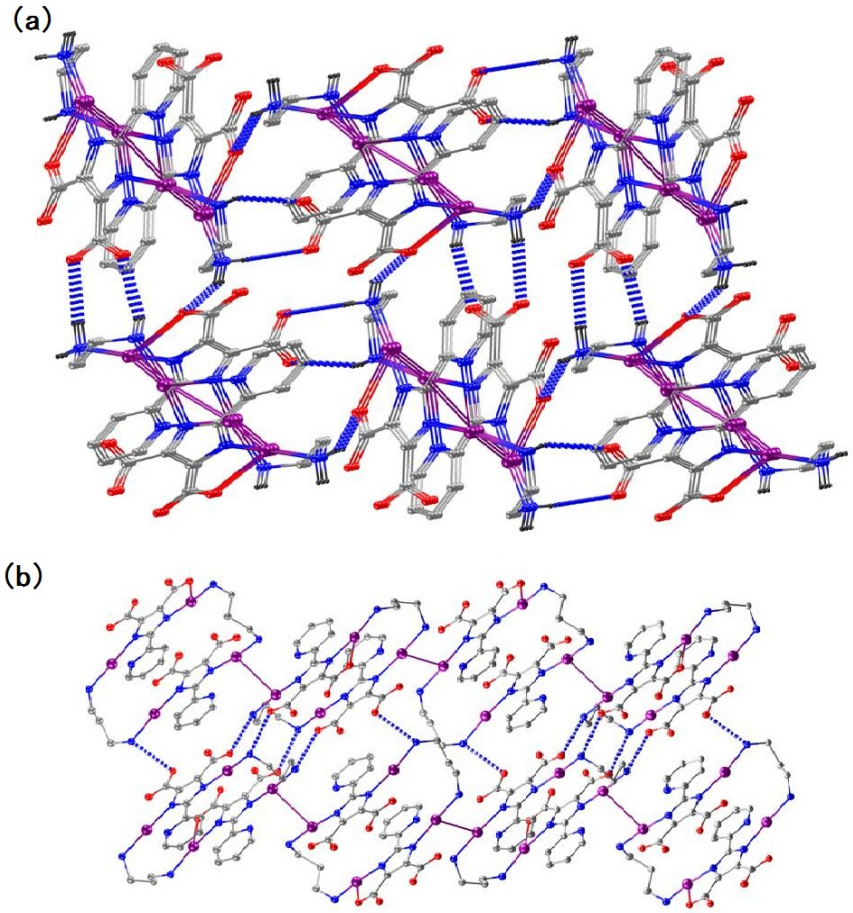

Fig. S5 The packing view of **3** (a) and **4** (b) through hydrogen bonds.

Physical Measurement Section

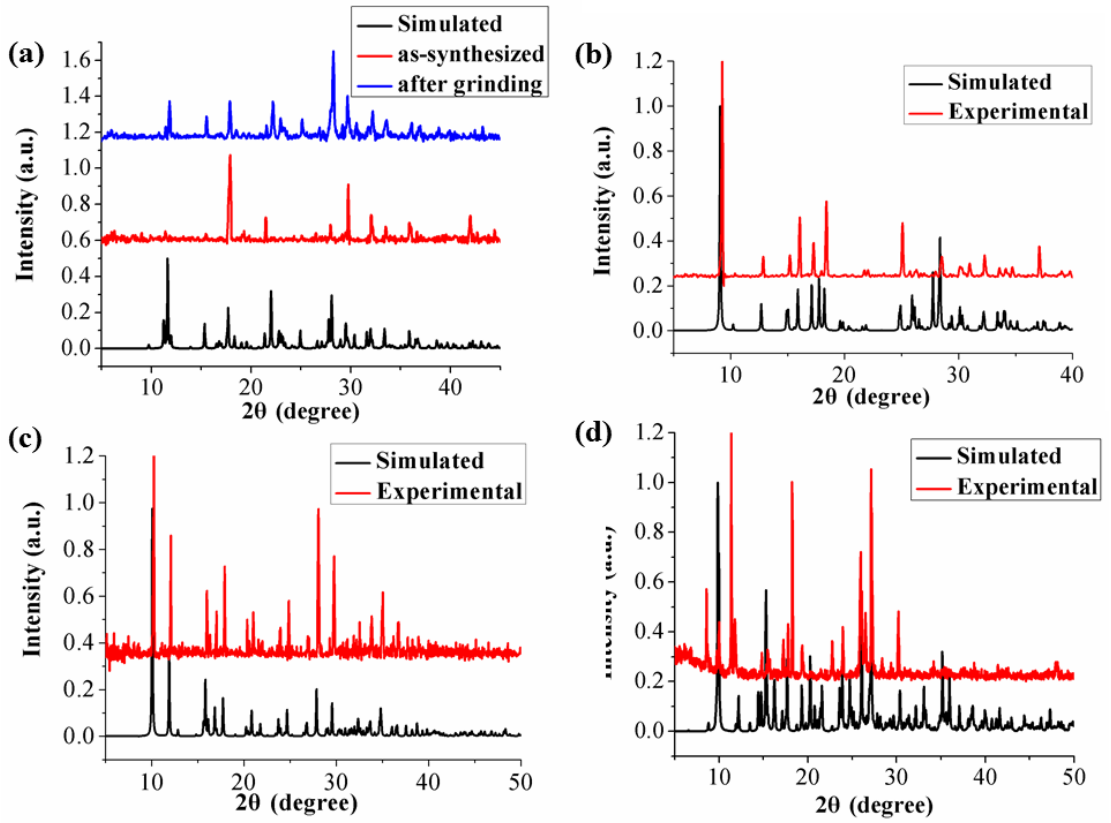

Fig. S6 Simulated (black) and experimental (red for as-synthesized and blue for after grinding) PXRD patterns of **1** (a), **2** (b), **3** (c) and **4** (d).

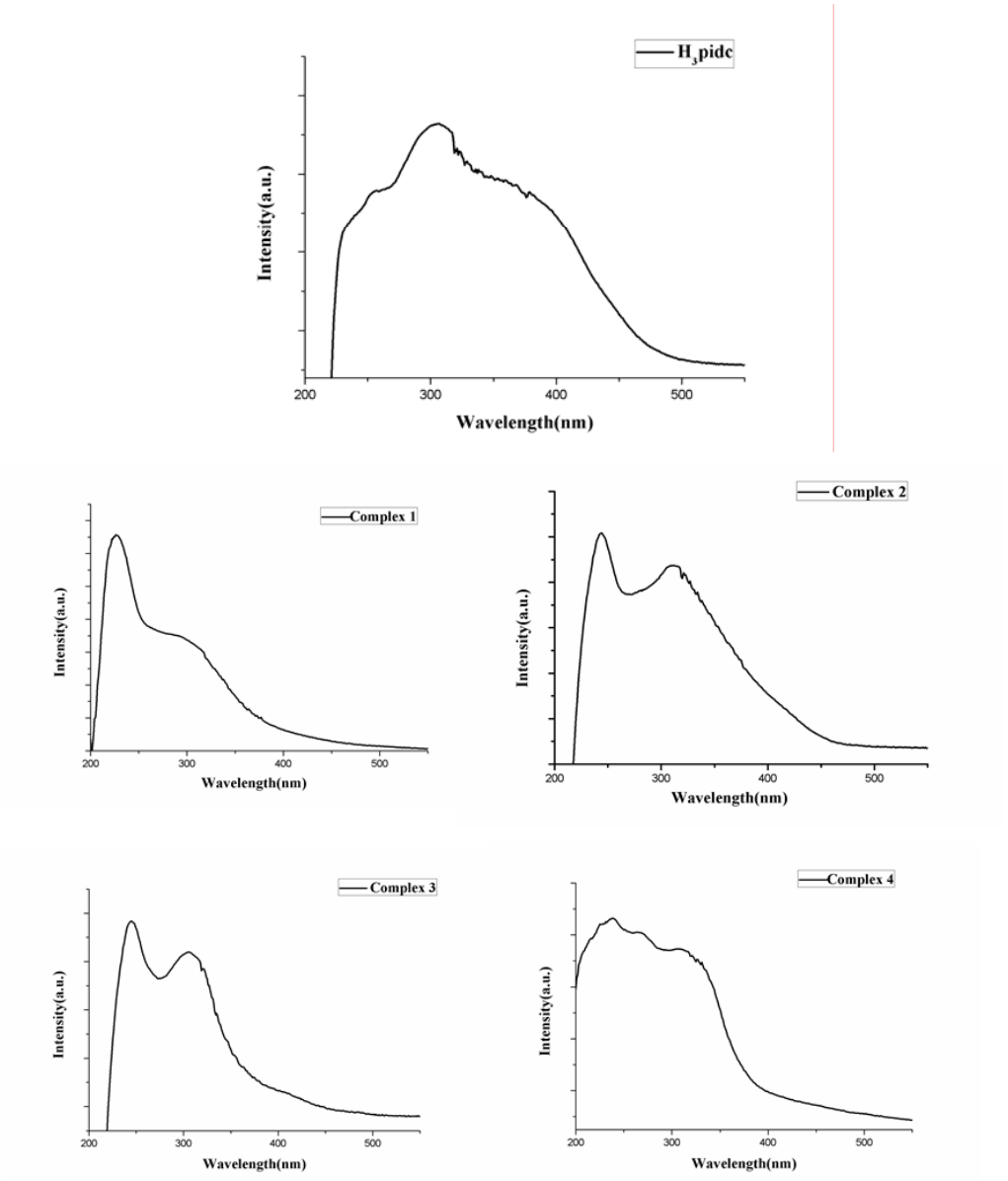

Fig. S7 The room-temperature solid state UV-Vis absorption spectra of H_3pidc and complex **1 – 4.**

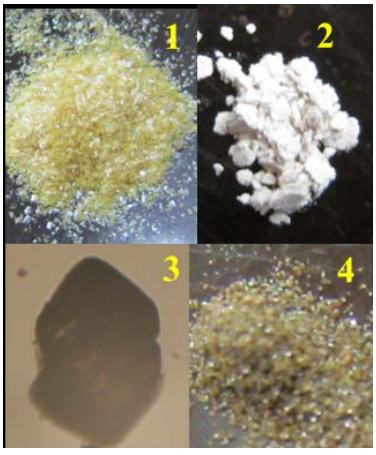

Fig. S8 The photographs of complex **1 – 4** under ambient light.

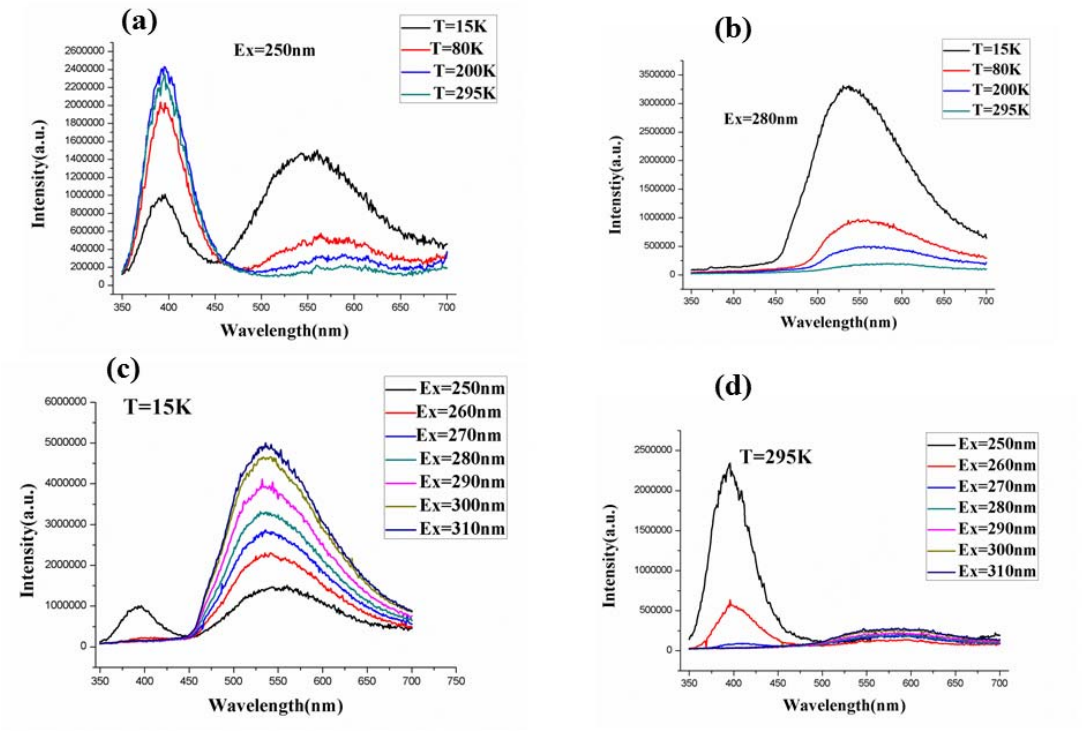

Fig. S9 The temperature-dependant solid state photoluminescent spectra of **1** at (a) different temperature upon λ_{ex} = 250 nm; (b) different temperature upon λ_{ex} = 280 nm; (c) 15 K upon different excitation light; (d) 295 K upon different excitation light.

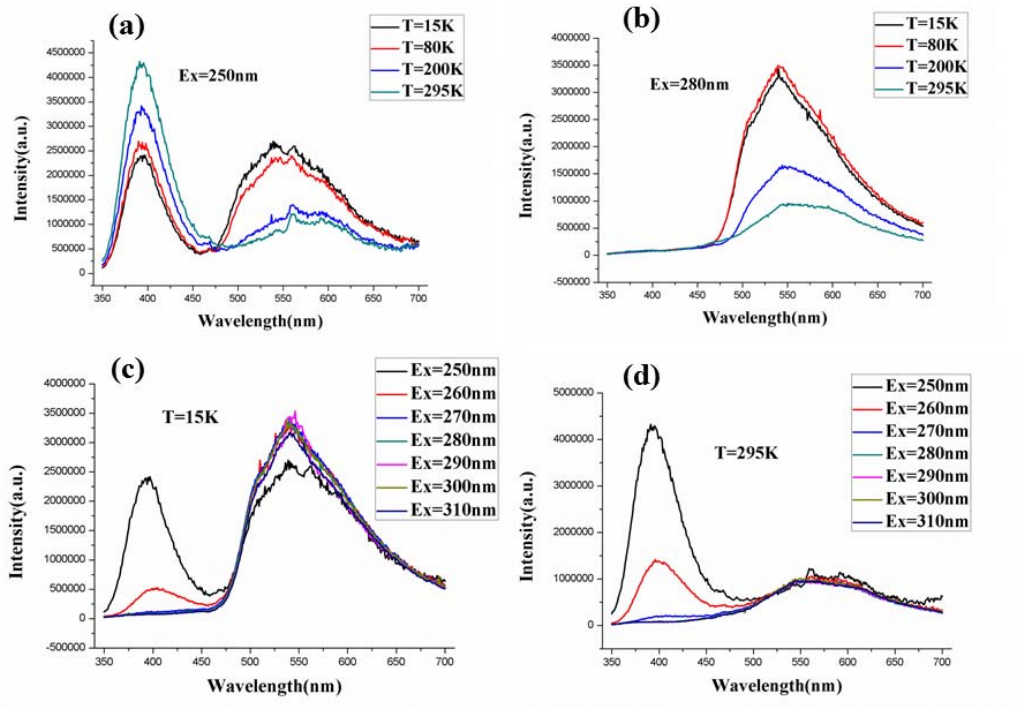

Fig. S10 The temperature-dependant solid state photoluminescent spectra of **2** at (a) different temperature upon λ_{ex} = 250 nm; (b) different temperature upon λ_{ex} = 280 nm; (c) 15 K upon different excitation light; (d) 295 K upon different excitation light.

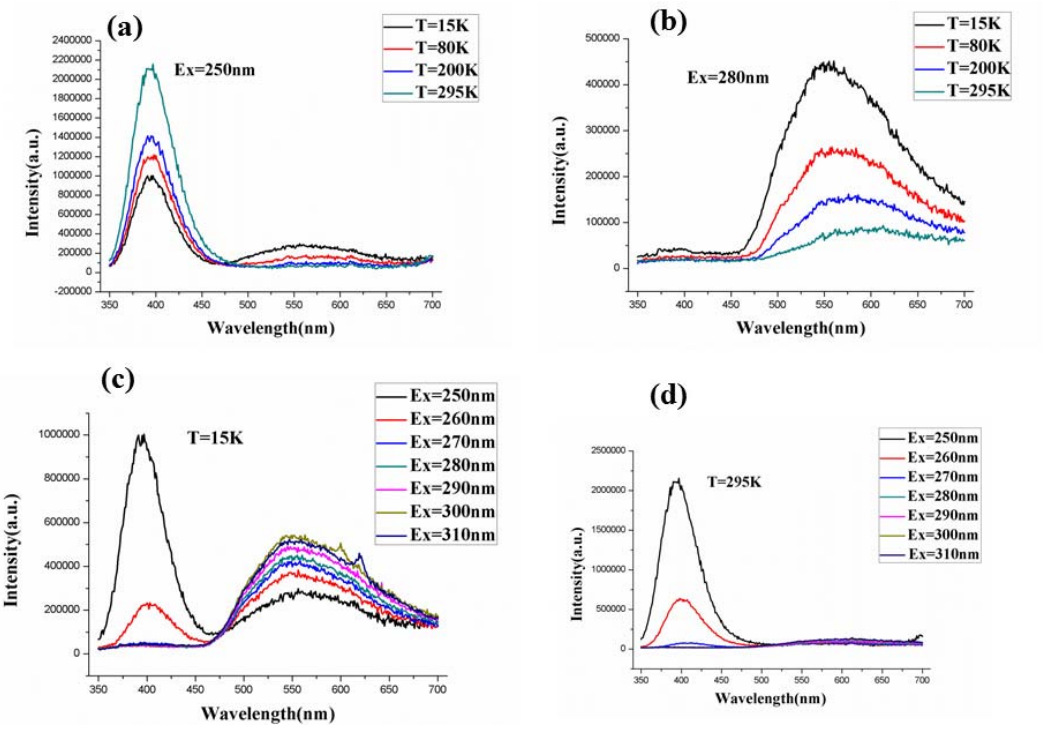

Fig. S11 The temperature-dependant solid state photoluminescent spectra of **3** at (a) different temperature upon λ_{ex} = 250 nm; (b) different temperature upon λ_{ex} = 280 nm; (c) 15 K upon different excitation light; (d) 295 K upon different excitation light.

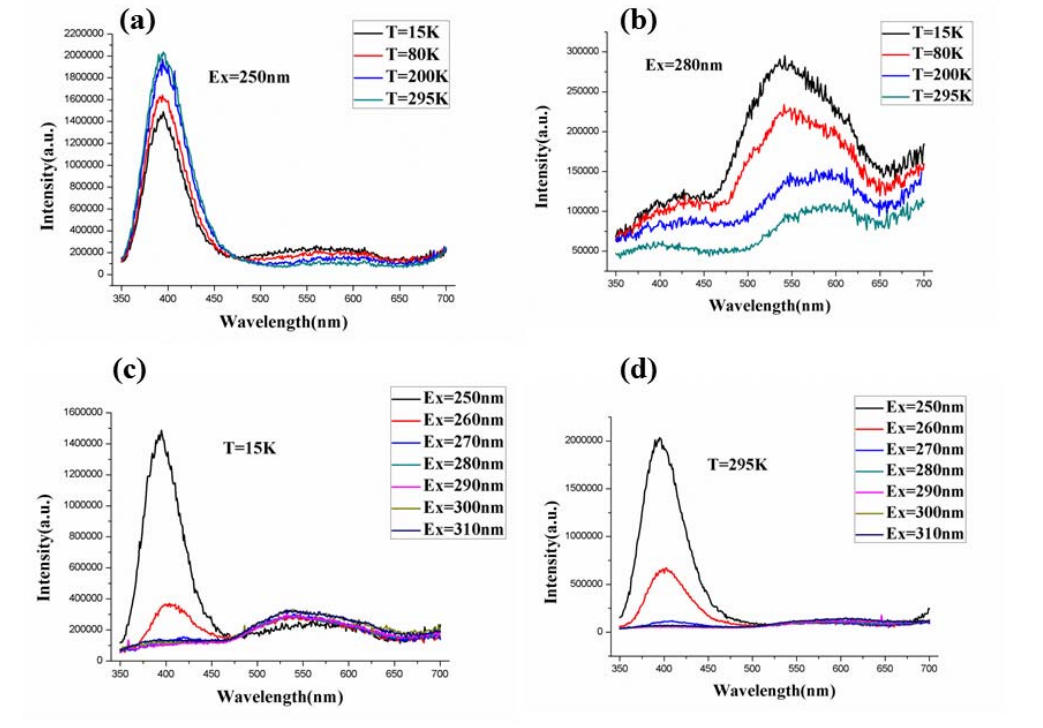

Fig. S12 The temperature-dependant solid state photoluminescent spectra of **4** at (a) different temperature upon λ_{ex} = 250 nm; (b) different temperature upon λ_{ex} = 280 nm; (c) 15 K upon different excitation light; (d) 295 K upon different excitation light.

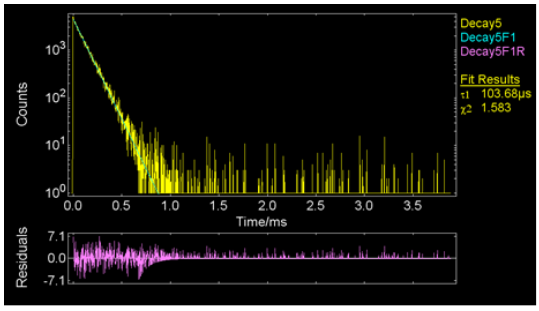

(a) T = 295 K, λ_{ex} = 250 nm, λ_{em} = 400 nm

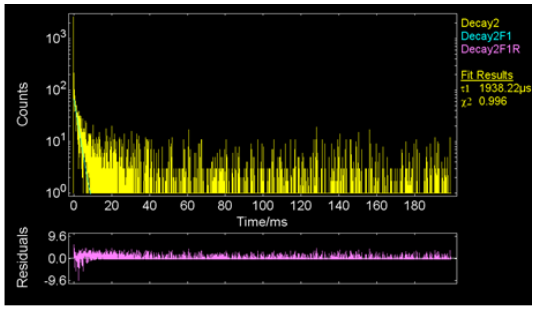

(b) T = 295 K, λ_{ex} = 260 nm, λ_{em} = 580 nm

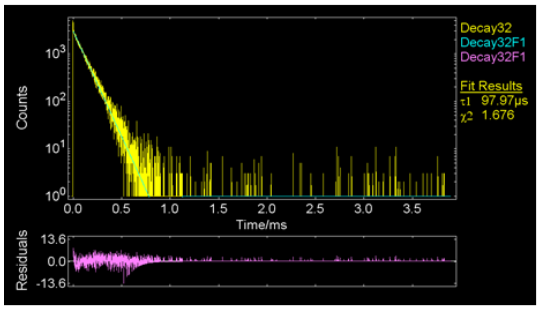

(c) T = 15 K, λ_{ex} = 250 nm, λ_{em} = 400 nm

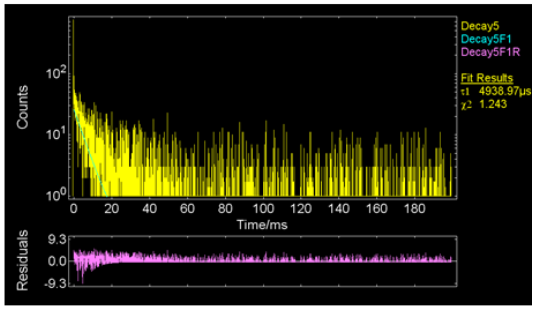

(d) T = 15 K, λ_{ex} = 260 nm, λ_{em} = 540 nm

Fig. S13 Selected luminescence decay of **1** monitored at corresponding excitation/emission maxima at 15 K and 295 K.

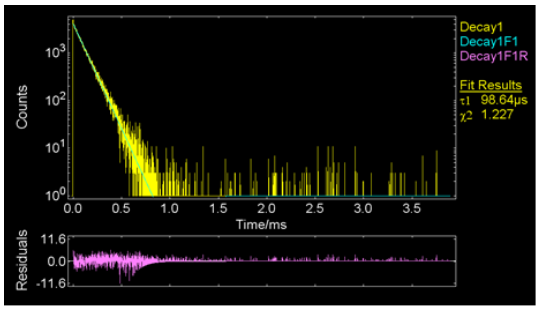

(a) T = 295 K, λ_{ex} = 250 nm, λ_{em} = 400 nm

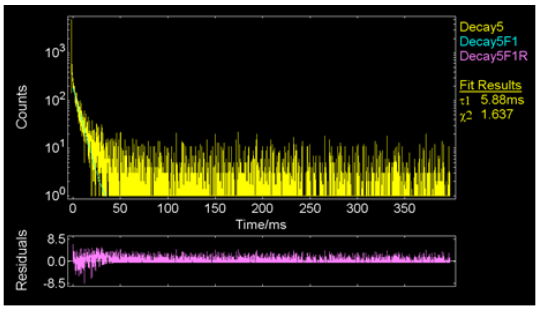

(b) T = 295 K, λ_{ex} = 270 nm, λ_{em} = 560 nm

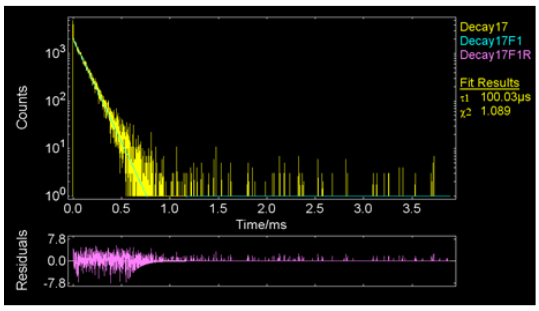

(c) T = 15 K, λ_{ex} = 250 nm, λ_{em} = 400 nm

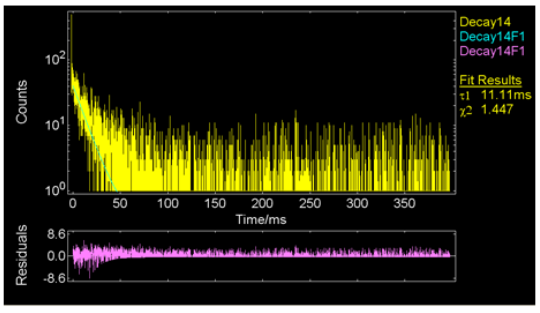

(d) T = 15 K, λ_{ex} = 260 nm, λ_{em} = 540 nm

Fig. S14 Selected luminescence decay of **2** monitored at corresponding excitation/emission maxima at 15 K and 295 K.

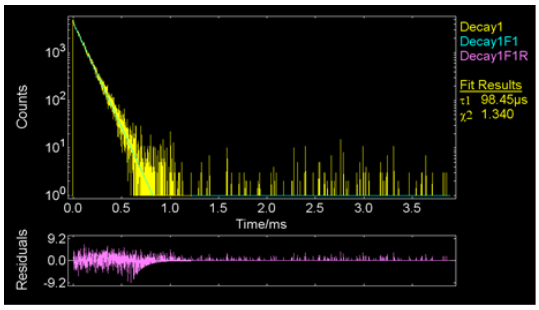

(a) $T = 295$ K, $\lambda_{ex} = 250$ nm, $\lambda_{em} = 400$ nm

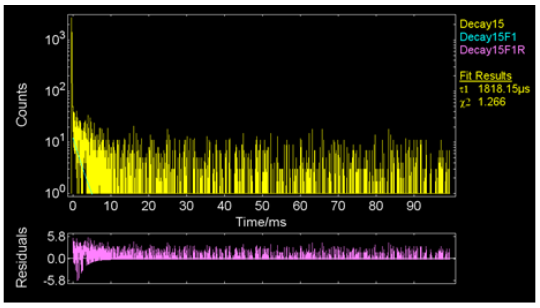

(b) $T = 295$ K, $\lambda_{ex} = 260$ nm, $\lambda_{em} = 600$ nm

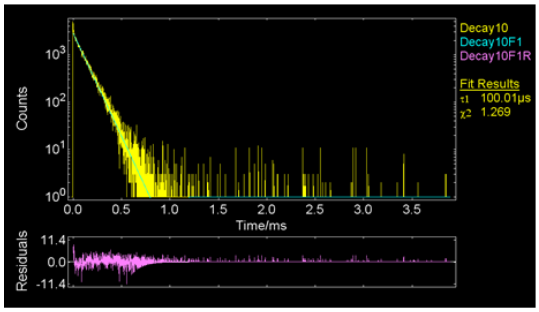

(c) $T = 15$ K, $\lambda_{ex} = 250$ nm, $\lambda_{em} = 400$ nm

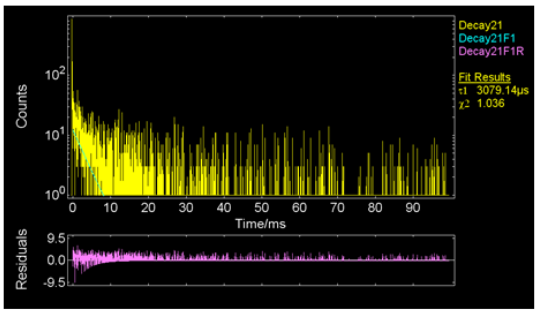

(d) $T = 15$ K, $\lambda_{ex} = 260$ nm, $\lambda_{em} = 540$ nm

Fig. S15 Selected luminescence decay of **3** monitored at corresponding excitation/emission maxima at 15 K and 295 K.

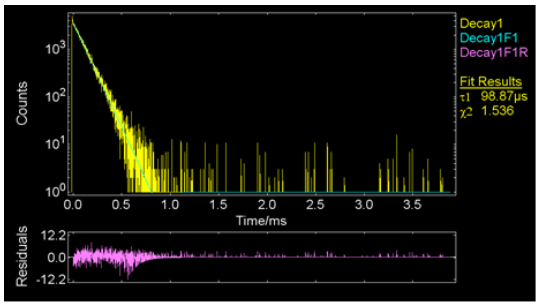

(a) $T = 295$ K, $\lambda_{ex} = 250$ nm, $\lambda_{em} = 400$ nm

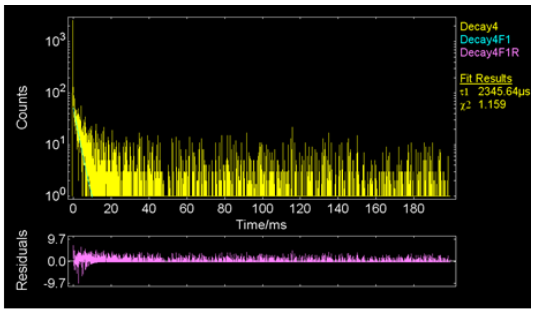

(b) $T = 295$ K, $\lambda_{ex} = 260$ nm, $\lambda_{em} = 600$ nm

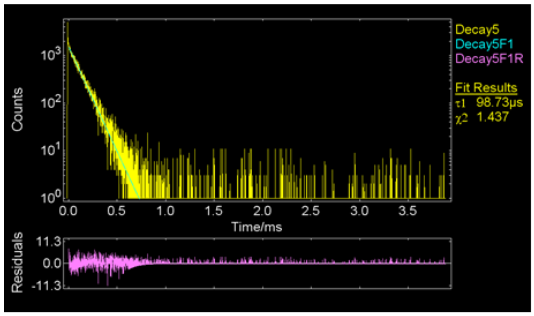

(c) $T = 15$ K, $\lambda_{ex} = 250$ nm, $\lambda_{em} = 400$ nm

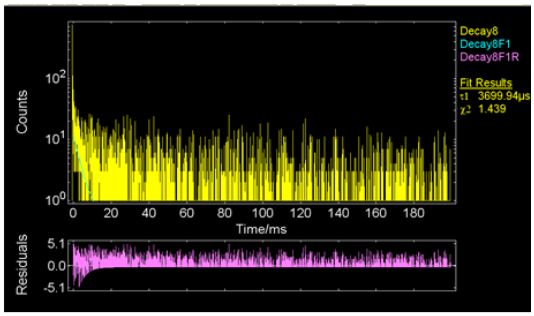

(d) $T = 15$ K, $\lambda_{ex} = 260$ nm, $\lambda_{em} = 540$ nm

Fig. S16 Selected luminescence decay of **4** monitored at corresponding excitation/emission maxima at 15 K and 295 K.

Table S7 Lifetimes (τ) of corresponding high energy emission (HE) peaks and low energy emission (LE) peaks for **1-4** in solid-state at 15 K and 295 K, respectively.

	HE (τ/μs)			LE (τ/ms)			
	λ (nm)	15 K	295 K	λ (nm)	15 K	λ (nm)	295 K
1	400	97.97	103.68	540	4.94	580	1.94
2	400	100.03	98.64	540	11.11	560	5.88
3	400	100.01	98.45	600	3.08	600	1.82
4	400	98.73	98.87	540	3.70	600	2.34

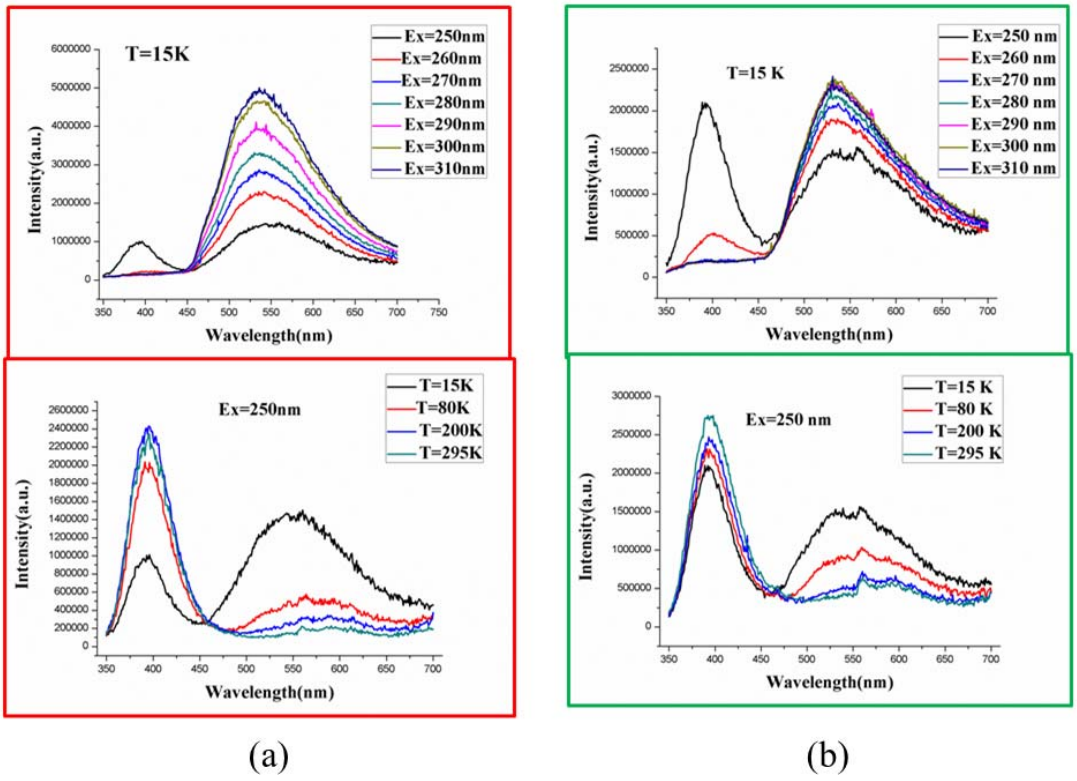

Fig. S17 The temperature-dependant luminescent spectra of **1** (a) before grinding and (b) after grinding.

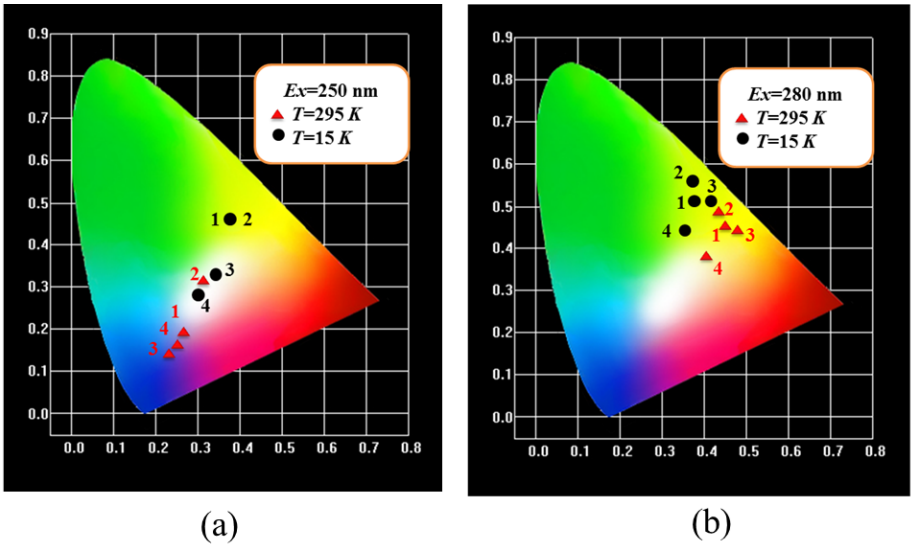

Fig. S18 The emission color profiles in CIE-1931 (Commission Internationale d'Eclairage) chromaticity diagram based on the temperature-dependant luminescent spectra for **1-4** when excited by 250 nm light (a) and 280 nm light (b) at 15 K and 295 K.

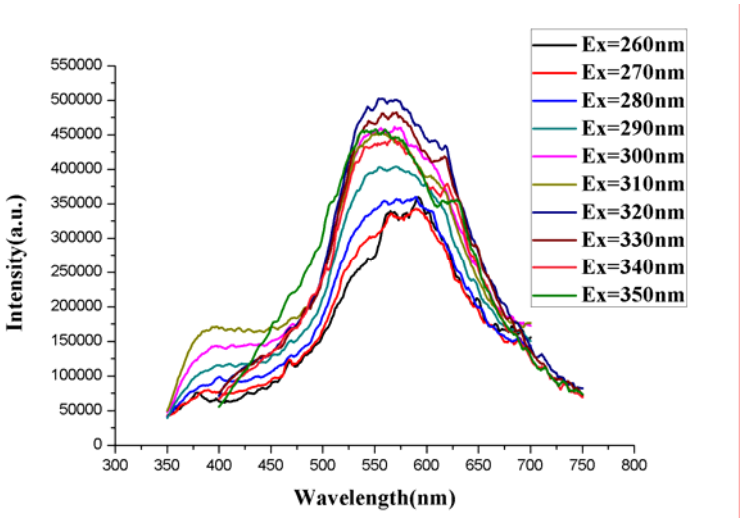

Fig. S19 The room temperature solid state photoluminescent spectrum of **1** upon excitation light of various wavelengths when exposure to air.

DFT Calculation Section

Computation details

Density functional theory (DFT) and time-dependent DFT (TD-DFT) calculations were performed using PBE0 functional.[S1] The Lanl2dz[S2] effective core potential (ECP) was used for Ag, while the 6-31G(d,p)[S3] basis set was applied for C, N, O, and H atoms. The UV-Vis spectra were simulated by TD-DFT[S4] and the first 50 lowest energy singlet-singlet spin-allowed excited states were calculated for binuclear molecule for **1**, dimer of binuclear molecules for **2**, and trtranuclear molecules for **3** and **4**. The simulated UV-Vis absorption data were further treated with

SWizard 4.6 [S5,S6] to give Table S8 – S11. In the TD-DFT calculation for **1** was based on its optimized geometry of S_0 state and the frequency calculation confirmed that it's the energy minimum geometry. In the TD-DFT calculations for **2-4** were all based on the tetranuclear units taken from their crystal structures at 298 K. The trials of optimizing these tetranuclear models were time-consuming and often leads to the unacceptable structural distortions despite of the selection of functional (PBE0, B3LYP, BLYP, M06, etc.) and basis set (Lanl2dz for all the atoms or Lanl2dz for Ag and 6-31g** for C, N, O, H, etc.), indicating the interdimer interaction for **2** and intermolecular interactions for **3** and **4** are quite strong. However, the low energy parts of experimental UV-Vis spectra **1-4** were qualitatively simulated, suggesting that our calculation method and calculation models were qualitatively correct. The discussions of the assignments of absorption transitions, only the molecular orbitals based on above models are taken into consideration, and the MBO was calculated based on the same models. Nevertheless, in order to looking for the insight of low energy emission bands, the molecular orbital calculations of S_0 state were carried out for the dimers for **1** and **2** taken from the crystal structures at 298 K and 100 K, respectively, as well as the tetranuclear units by considering two adjacent molecules for **3** and **4**. The SOMOs of T_1 states of all the above calculation models were also calculated by UPBE0 without optimizations, but the SOMOs of T1 state of binuclear molecule for **1** was calculated after optimized by UPBE0. The molecular orbital compositions were analyzed mainly by Hirshfeld method.[S7, S8] The compositions of occupied molecular orbitals (excluding singly occupied molecular orbitals, SOMOs) were also calculated by the natural atomic orbital (NAO) method[S9] using the NBO program (version 3.1)[S10] as included in Gsussian 09. The composition data from both methods and Mayer bond order (MBO)[S11] were obtained using MultiWFN 2.6.1[S12]. The Gaussian 09 A. 02 software package[S13] was used for all calculations.

The assignment analysis of low energy absorption band for complex 1-4

There are strong low energy absorption band centered at 300 nm – 325 nm for H_3pidc and **1-4**, and it seems that these low energy bands should only arise from intraligand (Hpidc2-) π-π or n-π transitions. However, the TD-DFT result show that Ag atoms play significant roles in the transitions involved in the low energy absorption bands.

The low energy parts of experimental UV-Vis spectra (not shorter than 280 nm for **1-3** and not shorter than 300 nm for **4**) of **1-4** were qualitatively simulated, suggesting that our calculation method and calculation models were qualitatively correct. We assign the origins of low energy band by the assignments of transitions of the simulated strongest absorption wavelength in this region.

The calculated strongest absorption peaks for **1** (λ = 310.6 nm, f = 0.1985) arise from the following transitions: HOMO-1→LUMO (67%), HOMO→LUMO+1(18%), HOMO→LUMO+2(7%), which should be mainly ^{1}ILCT centred at Hpidc^{2-} with some contributions of ^{1}LMCT from Hpidc^{2-} to Ag and ^{1}LLCT from Hpidc^{2-} to auxiliary amine ligand.

The calculated strongest absorption peaks for **2** (λ = 284.1 nm, f = 0.0925) arise from the following transitions: H-2→L+5 (34%), H-7→L+3 (21%), H-2→L+6 (17%), H-5→L+3 (15%), which should be mainly ^{1}ILCT mixed with ^{1}LMMCT from Hpidc^{2-} to Ag-Ag bond and ^{1}LLCT.

The calculated strongest absorption peaks for **3** (λ = 299.9 nm, f = 0.1554) arise from the following transition: H-3→L+1 (82%), which should be mainly ^{1}ILCT mixed with ^{1}LMMCT from Hpidc^{2-} to Ag-Ag bond and ^{1}LLCT.

In summary of this part, the low energy strong absorption bands for **1-4** are assigned as ^{1}ILCT with some contributions from ^{1}LMCT (or ^{1}LMMCT) and ^{1}LLCT.

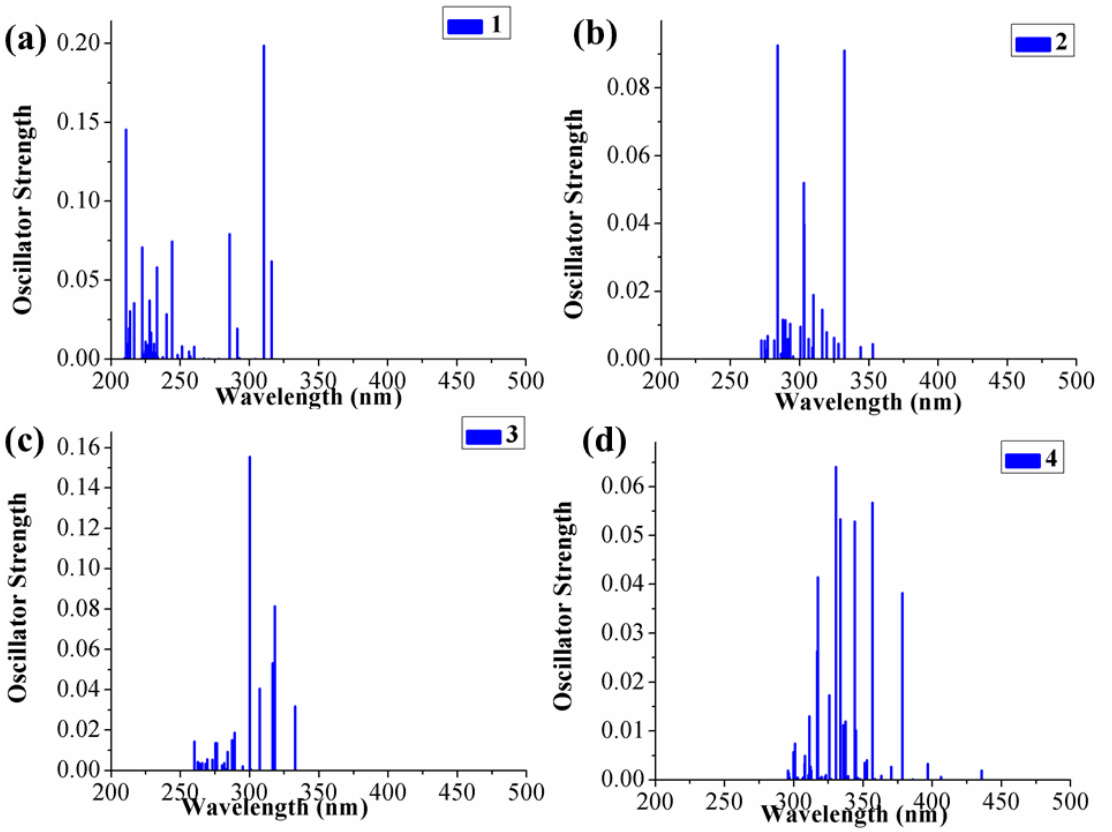

Fig. S20 The simulated UV-Vis absorption spectra of (a) complex **1**, (b) complex **2**, (c) complex **3**, (d) complex **4**.

Table S8 First 50 lowest energy singlet-singlet excitation for complex **1** by TD-DFT.

No.	nm	oscillator strength	Assignment(H=HOMO,L=LUMO)
1	332.3	0.0000	H→L (93%)
2	316.1	0.0619	H→L+1 (70%), H-1→L (22%)
3	310.6	0.1985	H-1→L (67%), H→L+1(18%), H→L+2(7%)
4	304.3	0.0001	H-1→L+1 (96%)
5	293.0	0.0007	H→L+3 (66%), H→L+4 (17%), H→L (10%)
6	291.4	0.0194	H→L+2 (75%), H-2→L+2 (7%)
7	285.6	0.0004	H-1→L+2 (96%)
8	285.5	0.0792	H-1→L+3 (91%)
9	277.9	0.0002	H-2→L (44%), H→L+3 (25%), H→L+4 (17%), H-3→L (5%)
10	270.8	0.0001	H-3→L (56%), H-5→L (19%), H→L+4 (15%)
11	266.9	0.0004	H-2→L (42%), H→L+4 (35%), H-3→L (11%)
12	260.0	0.0079	H-2→L+1 (80%), H-3→L+1(10%)
13	257.3	0.0017	H-4→L+1 (90%)
14	256.4	0.0050	H-4→L (94%)
15	256.2	0.0001	H-5→L (43%), H-2→L+4 (15%), H-3→L (12%), H-2→L+3 (10%)
16	251.1	0.0080	H-3→L+1 (84%), H-2→L+1 (9%)
17	248.9	0.0003	H-2→L+3 (42%), H-5→L (14%), H-2→L+4 (12%), H-3→L (5%)
18	248.0	0.0028	H-2→L+2 (65%), H-3→L+2 (17%), H→L+2(11%)

19	246.1	0.0000	H-3→L+3(44%), H-3→L+4 (27%)
20	243.9	0.0747	H-1→L+4 (76%), H-6→L (13%)
21	240.2	0.0285	H-3→L+2 (49%), H-5→L+2 (25%), H-2→L+2 (15%)
22	237.3	0.0012	H-2→L+4 (25%), H-3→L+4 (24%), H-5→L+3 (15%), H→L+5 (9%)
23	234.6	0.0002	H→L+5 (70%)
24	233.3	0.0021	H-2→L+3 (40%), H-2→L+4 (20%), H-5→L+3 (11%), H-3→L+4 (7%)
25	233.1	0.0583	H-6→L (46%), H-8→L+1 (13%), H-1→L+4 (10%), H-3→L+2 (9%), H-7→L (8%)
26	231.7	0.0038	H-4→L+3 (53%), H-1→L+5 (28%), H-8→L+1 (10%)
27	231.3	0.0007	H-4→L+2 (81%), H-6→L+2 (6%)
28	231.0	0.0097	H-8→L (58%), H-9→L (10%), H-4→L+2 (7%)
29	230.7	0.0047	H-1→L+5 (50%), H-4→L+3 (38%), H-8→L+1 (5%)
30	228.9	0.0166	H-5→L+2 (38%), H-5→L+1 (14%), H-3→L+2 (13%), H-6→L (10%), H→L+6 (7%), H-8→L+1 (5%)
31	228.7	0.0001	H-6→L+1 (60%), H-7→L+1 (21%)
32	227.8	0.0372	H-8→L+1 (43%), H-5→L+2 (15%), H-1→L+5 (15%), H→L+6 (9%)
33	226.0	0.0091	H→>L+6 (52%), H-6→L (13%), H-5→L+1(10%), H-7→L (7%)
34	225.6	0.0001	H-1→L+6 (92%)
35	224.9	0.0110	H→L+7 (55%), H-3→L+3 (9%), H-2→L+5 (7%), H-5→L+3 (7%)
36	224.6	0.0052	H-5→L+1 (68%), H→L+6 (10%), H-5→L+2 (9%)
37	223.9	0.0029	H-3→L+3 (27%), H-5→L+3 (19%), H-3→L+4 (13%), H→L+7 (13%), H-8→L (5%)
38	222.5	0.0707	H-7→L (63%), H→L+6 (10%), H-1→L+7 (9%), H-6→L(5%)
39	221.5	0.0002	H-9→L (56%), H-8→L (18%), H-5→L (5%)
40	218.7	0.0000	H-6→L+2 (75%), H-4→L+2 (7%), H-7→L+2 (5%)
41	216.6	0.0355	H-1→L+7 (60%), H-6→L+3 (21%), H-7→L (8%)
42	213.7	0.0303	H-6→L+3 (44%), H-1→L+7 (22%), H-7→L+3 (10%), H→L+8 (6%)
43	213.2	0.0007	H-7→L+1 (51%), H-7→L+2 (30%), H-6→L+1 (14%)
44	212.7	0.0197	H-10→L (44%), H-4→L+4 (20%), H-11→L+3 (10%)
45	212.1	0.0099	H-4→L+4 (34%), H→L+8 (32%), H-10→L (13%)
46	211.5	0.0015	H-7→L+2 (48%), H-7→L+1 (17%), H-6→L+2 (10%), H-6→L+1 (9%), H-1→L+8 (8%)
47	210.7	0.1456	H-4→L+4 (33%), H→L+8 (27%), H-6→L+3(9%)
48	210.7	0.0000	H-1→L+8 (78%), H-7→L+2 (6%)
49	210.3	0.0004	H-5→L+4 (28%), H-8→L+3 (28%), H-5→L+3 (11%), H-9→L+3 (11%), H-1→L+8 (7%)
50	209.6	0.0005	H→L+9 (80%), H→L+8 (6%)

Table S9 First 50 lowest energy singlet-singlet excitation for complex **2** by TD-DFT.

No.	nm	oscillator strength	Assignment (H=HOMO,L=LUMO)
1	352.8	0.0008	H→L (46%), H-1→L+1 (33%), H→L+1 (7%), H-1→L (7%)
2	352.8	0.0044	H-1→L (46%), H→L+1 (34%), H→L (7%), H-1→L+1 (7%)

3	344.3	0	H-1→L+2 (38%), H-1→L+1 (36%), H→L (18%)
4	344	0.0035	H→L+2 (38%), H→L+1 (35%), H-1→L (17%), H-1→L+3 (6%)
5	332.4	0.0911	H-2→L+1 (80%), H-2→L+2 (13%)
6	330.3	0	H-2→L (87%)
7	328.6	0	H→L+3 (73%), H-2→L (6%)
8	328	0.0046	H-1→L+3 (78%)
9	325.1	0.0001	H-1→L+2 (48%), H→L (21%), H-1→L+1 (17%)
10	324.9	0.0063	H→L+2 (51%), H-1→L (22%), H→L+1 (15%)
11	321.7	0	H-3→L+1 (61%), H-2→L+3 (16%), H-3→L+2 (12%)
12	319.5	0.0079	H-2→L+2 (78%), H-2→L+1 (14%)
13	318.4	0	H-2→L+3 (75%), H-3→L+1 (8%)
14	316.4	0.0146	H-3→L (88%)
15	311.4	0	H-4→L (45%), H-5→L+1 (14%), H-3→L+2 (14%), H-7→L+1 (8%), H-6→L (7%), H-3→L+1 (6%)
16	310	0.019	H-5→L (45%), H-6→L+1 (23%), H-4→L+1 (14%)
17	309.2	0.0034	H-4→L+1 (32%), H-7→L (26%), H-6→L+1 (12%), H→L+5 (8%), H-1→L+8 (7%)
18	309.1	0	H-5→L+1 (21%), H-6→L (20%), H-7→L+1 (16%), H-4→L (10%), H→L+8 (9%), H-1→L+5(8%)
19	306.7	0.0006	H→L+8 (22%), H-1→L+5 (17%), H-5→L+1 (13%), H→L+3 (8%), H-7→L+1 (7%), H-1→L+9 (7%)
20	306.6	0.006	H-1→L+8 (21%), H→L+5 (18%), H-6→L+1 (12%), H-1→L+3 (8%), H→L+9 (7%), H-4→L+1 (5%)
21	305.9	0	H-3→L+2 (54%), H-7→L+1 (18%), H-3→L+1 (9%), H-5→L+1 (6%)
22	303.4	0.0399	H-7→L (31%), H-3→L+3 (26%), H-4→L+2 (22%), H-4→L+1(9%)
23	303.4	0	H-6→L (37%), H-7→L+2 (12%), H-5→L+2 (12%), H-4→L (7%), H-7→L+1 (7%)
24	302.9	0.052	H-3→L+3 (35%), H-6→L+2 (19%), H-5→L (17%), H-7→L(7%)
25	300.8	0	H-5→L+2 (24%), H-7→L+1 (17%), H-7→L+2 (14%), H-4→L (11%), H-5→L+1 (10%), H-4→L+3(7%), H-6→L (6%), H-3→L+1 (6%)
26	300.5	0.0096	H-6→L+1 (23%), H-4→L+2 (15%), H-5→L+3 (13%), H-4→L+1 (11%), H-5→L (11%), H-3→L+3 (10%), H-6→L+2 (10%)
27	295.5	0	H→L+4 (25%), H-1→L+6 (23%), H-6→L+3 (19%), H-4→L+3 (14%)
28	295.2	0.0008	H-1→L+4(37%), H→L+6 (33%), H-7→L+3 (9%), H-1→L+7 (7%)
29	294.1	0	H→L+4 (25%), H-6→L+3 (24%), H-4→L+3 (15%), H-1→L+6 (12%)
30	293.2	0.0105	H-7→L+3 (36%), H-5→L+3 (21%), H-1→L+4 (14%)
31	291.5	0.006	H-6→L+2(24%), H-7→L (16%), H-4→L+2 (16%), H-8→L (8%), H-4→L+1 (7%), H-6→L+1 (5%)
32	291.3	0	H-7→L+2(33%), H-5→L+2 (17%), H-7→L+1(10%), H-6→L (9%)
33	289.7	0.0001	H-1→L+5 (33%), H→L+7 (24%), H→L+4 (12%), H→L+8 (10%), H-1→L+9 (6%)
34	289.6	0.0115	H→L+5 (29%), H-1→L+7 (22%), H-1→L+4 (9%), H-1→L+8 (8%), H→L+9 (5%)

35	287.7	0.0116	H-5→L+3 (25%), H-2→L+5 (17%), H-7→L+3 (13%), H-2→L+6 (12%), H-4→L+1 (6%)
36	286.9	0	H-5→L+2 (21%), H-4→L (14%), H-5→L+1 (13%), H-4→L+3 (11%), H-7→L+2 (9%), H-6→L (9%), H-6→L+3 (7%), H-7→L+1 (6%)
37	286.4	0.0016	H-4→L+2(32%), H-6→L+2 (24%), H-5→L (12%),H-7→L (6%)
38	286.1	0	H-4→L+3 (41%), H-6→L+3 (24%), H-7→L+2 (13%), H-5→L+2 (11%)
39	284.1	0.0925	H-2→L+5 (34%), H-7→L+3 (21%), H-2→L+6 (17%), H-5→L+3 (15%)
40	282.8	0	H-2→L+4 (68%), H-1→L+6 (8%), H-2→L+7 (6%)
41	281.6	0.0056	H→L+6 (42%), H-1→L+7 (26%), H-1→L+4 (10%)
42	281.4	0	H-1→L+6 (32%), H→L+7 (23%), H-2→L+4 (13%), H→L+4 (7%)
43	278.7	0	H-8→L+1 (36%), H-8→L+2 (12%), H-6→L+3 (9%), H-9→L+3 (7%)
44	276.8	0	H-3→L+5 (42%), H-3→L+6 (24%), H-8→L+1 (5%)
45	276.8	0.0068	H-9→L+1 (17%), H-8→L+3 (16%), H-9→L+2 (9%), H-6→L+5 (8%), H-1→L+4 (6%), H-7→L+8 (5%)
46	276.3	0.0027	H-2→L+6 (23%), H-1→L+7 (19%), H→L+5 (16%), H-2→L+5 (9%), H-1→L+8 (9%), H-1→L+4 (7%), H→L+6 (5%)
47	276.1	0	H→L+7 (23%), H-1→L+5 (17%), H→L+4 (12%), H→L+8 (10%), H-3→L+5 (8%), H-1→L+6 (7%), H-3→L+6 (5%)
48	274.8	0.0054	H-2→L+6 (36%), H-2→L+5 (20%), H-1→L+7 (7%), H-3→L+4 (6%), H→L+5 (6%), H-1→L+4 (5%), H-9→L+1 (5%)
49	273.3	0	H-2→L+7 (69%), H-2→L+4 (11%)
50	272.4	0.0055	H-3→L+4(50%), H-3→L+7(16%), H-8→L(9%)

Table S10 First 50 lowest energy singlet-singlet excitation for complex **3** by TD-DFT.

No.	nm	oscillator strength	Assignment(H=HOMO,L=LUMO)
1	332.7	0.0318	H→L (81%), H-2→L (7%), H-1→L+1(6%)
2	329.1	0.0000	H-1→L (65%),H→L+1 (23%)
3	321.7	0.0000	H→L+1 (58%),H-1→L (29%)
4	318.2	0.0815	H-1→L+1 (39%), H-2→L (17%), H→L (14%), H-1→L+8 (6%), H→L+4 (6%)
5	316.5	0.0532	H-2→L (64%), H-1→L+1 (28%)
6	312.7	0.0000	H-3→L (71%), H-2→L+1 (12%), H→L+1 (7%)
7	311.4	0.0000	H-2→L+1 (51%), H-3→L (23%)
8	307.1	0.0406	H→L+4 (27%), H-1→L+1 (18%), H-1→L+8 (16%), H-2→L+4 (10%), H-2→L (6%)
9	305.9	0.0000	H-1→L+4 (26%), H-2→L+1 (25%), H→L+8 (14%), H-2→L+8 (9%), H-1→L+6 (5%)
10	301.5	0.0000	H→L+2 (65%), H-1→L+3 (16%)
11	301.1	0.0006	H→L+3 (58%), H-1→L+2 (25%)
12	299.9	0.1554	H-3→L+1 (82%)

13	294.9	0.0021	H-1→L+2 (34%), H-2→L+3 (29%), H→L+3(26%)
14	294.7	0.0000	H-2→L+2 (34%), H-1→L+3 (33%), H→L+2(20%)
15	290.3	0.0000	H-4→L (73%), H-5→L+1(15%)
16	289.1	0.0188	H-5→L (67%), H-4→L+1 (21%)
17	288.9	0.0000	H→L+5 (36%), H-7→L (28%), H-2→L+2 (6%)
18	288.0	0.0045	H-6→L (60%), H-8→L+1 (6%), H-1→L+5 (5%)
19	287.4	0.0151	H→L+4 (30%), H-2→L+4 (28%), H-2→L+3 (14%), H-3→L+2 (8%), H-1→L+2 (6%)
20	287.0	0.0000	H-7→L (27%), H-2→L+2 (18%), H→L+5 (17%), H-1→L+3 (9%), H-3→L+3 (7%)
21	284.6	0.0000	H-1→L+3 (26%), H-2→L+2 (22%), H→L+5 (18%), H-7→L (11%), H→L+7 (8%)
22	284.2	0.0092	H-2→L+3 (36%), H-1→L+2 (19%), H→L+4 (9%), H-6→L(6%)
23	282.4	0.0000	H-6→L+1 (42%), H-3→L+3 (16%), H-7→L (7%), H-8→L (6%)
24	282.2	0.0009	H-7→L+1 (42%), H-4→L+1 (12%), H-1→L+5 (8%), H-3→L+2 (7%), H-9→L (5%)
25	281.7	0.0039	H-1→L+5 (48%), H-6→L(9%), H→L+4 (7%), H-1→L+2 (6%), H→L+6 (5%), H-2→L+6 (5%)
26	281.3	0.0000	H-3→L+3 (31%), H-2→L+5 (19%), H-6→L+1 (12%)
27	280.2	0.0027	H-3→L+2 (70%), H-7→L+1 (7%)
28	279.0	0.0000	H-1→L+4 (31%), H→L+8 (18%), H→L+7 (16%), H-3→L+4 (6%)
29	277.3	0.0000	H-2→L+5 (29%), H-3→L+3 (16%), H-2→L+7 (+14%), H-5→L+1 (10%), H-1→L+6 (7%)
30	276.3	0.0136	H-2→L+4 (26%), H-1→L+7 (17%), H-1→L+8 (16%), H→L+9 (6%), H-7→L+1 (6%)
31	275.5	0.0000	H→L+7 (35%), H-3→L+4 (31%), H-5→L+1 (12%), H→L+5 (6%)
32	275.4	0.0136	H-4→L+1 (60%), H-5→L (19%), H-7→L+1 (7%)
33	274.9	0.0000	H-5→L+1 (48%), H-4→L (14%), H-2→L+5 (11%), H-3→L+3 (7%)
34	273.2	0.0054	H→L+6 (46%), H-3→L+5 (18%), H-1→L+5 (12%)
35	271.2	0.0000	H-3→L+4 (28%), H→L+7 (16%), H-2→L+7 (13%), H-1→L+4 (6%), H-3→L+3 (5%), H-7→L+4 (5%)
36	269.6	0.0009	H-3→L+5 (47%), H→L+6 (9%), H-3→L+7 (9%), H-2→L+6 (7%), H-1→L+7 (5%)
37	269.3	0.0057	H-1→L+7 (27%), H-6→L+4 (16%), H-4→L+2 (12%), H-5→L+3 (8%), H-7→L+8 (8%)
38	268.4	0.0000	H-5→L+2 (34%), H-4→L+3 (32%)
39	268.0	0.0034	H-4→L+2 (38%), H-5→L+3 (26%), H-6→L+4 (6%), H-3→L+5 (5%)
40	267.9	0.0000	H-7→L+4 (16%), H-5→L+2 (14%), H-2→L+7 (13%), H-6→L+8 (12%), H-4→L+3 (10%), H-2→L+8 (5%), H-7→L+6 (5%)
41	266.2	0.0000	H-1→L+6 (42%), H-2→L+5 (16%), H-1→L+4 (7%), H→L+8 (6%), H-2→L+7 (5%)
42	265.8	0.0039	H-1→L+7 (17%), H-2→L+6 (16%), H-2→L+4 (14%), H-6→L+4 (9%), H-7→L+8 (8%)

43	265.6	0.0000	H-2→L+7 (30%), H-8→L (11%), H→L+8 (9%), H-6→L+8 (6%), H-3→L+4 (6%)
44	263.7	0.0036	H-2→L+6 (42%), H-1→L+7 (6%), H-9→L (6%)
45	263.6	0.0000	H-2→L+8 (33%), H→L+8 (21%), H-1→L+6 (9%), H-6→L+2 (8%)
46	263.4	0.0000	H-8→L (37%), H-6→L+1 (16%), H-9→L+1 (7%), H-1→L+6 (7%), H-2→L+7 (7%)
47	262.5	0.0042	H-8→L+1 (31%), H-9→L(19%), H-7→L+1 (13%), H-7→L+2 (5%)
48	260.2	0.0118	H-3→L+7 (48%), H-3→L+5 (9%), H-7→L+2 (9%), H-5→L+4 (5%)
49	260.1	0.0000	H-3→L+6 (24%), H-6→L+2 (23%), H-7→L+3 (12%), H-8→L+3 (10%)
50	260.0	0.0144	H-7→L+2 (41%), H-6→L+3 (27%)

Table S11 First 50 lowest energy singlet-singlet excitation for complex **4** by TD-DFT.

No.	nm	oscillator strength	Assignment(H=HOMO,L=LUMO)
1	461.4	0.0000	H→L (99%)
2	435.6	0.0019	H-1→L (89%), H-2→L (10%)
3	406.5	0.0006	H→L+2 (60%), H→L+1 (29%)
4	405.5	0.0000	H-4→L (78%), H-2→L (15%)
5	396.7	0.0033	H-2→L (73%), H-4→L (13%), H-1→L (9%)
6	385.8	0.0001	H-3→L (91%), H-4→L (6%)
7	380.0	0.0000	H→L+1 (66%), H→L+2 (32%)
8	378.4	0.0382	H-1→L+2 (51%), H-1→L+1 (26%), H-2→L+2 (6%)
9	370.5	0.0027	H→L+4 (49%), H→L+5 (27%), H→L+3 (8%)
10	363.1	0.0009	H-1→L+1 (59%), H-1→L+2 (24%), H-2→L+1 (7%)
11	358.4	0.0002	H→L+3 (86%), H→L+5 (5%)
12	356.7	0.0567	H-5→L (88%)
13	352.6	0.0041	H-2→L+2 (39%), H-2→L+1 (24%), H-1→L+4 (13%), H-1→L+2 (10%), H-1→L+5 (6%)
14	351.8	0.0023	H→L+6 (50%), H→L+4 (19%), H→L+5 (18%)
15	351.0	0.0035	H-3→L+2 (53%), H-3→L+1 (24%)
16	347.9	0.0002	H-7→L (87%)
17	346.2	0.0004	H→L+6 (37%), H→L+5 (36%), H→L+4 (20%)
18	344.7	0.0102	H-4→L+1 (67%), H-2→L+1 (10%), H-1→L+4 (8%)
19	344.2	0.0529	H-1→L+4 (37%), H-2→L+2 (11%), H-4→L+1 (11%), H-2→L+4 (6%)
20	339.3	0.0008	H-4→L+2 (79%), H-4→L+1 (6%)
21	337.3	0.0120	H-1→L+3 (32%), H-2→L+1 (18%), H-6→L (11%), H-1→L+2 (6%), H-2→L+2 (5%), H-8→L (5%)
22	335.8	0.0112	H-1→L+3 (49%), H-6→L (14%), H-2→L+1 (8%), H-8→L (7%), H-2→L+2 (6%)
23	333.8	0.0533	H-6→L (32%), H-2→L+1 (15%), H-2→L+2 (13%), H-8→L (13%), H-1→L+4 (7%), H-1→L+3 (6%)
24	330.6	0.0640	H-1→L+5 (57%), H-1→L+6 (12%), H-2→L+2 (5%)

25	326.9	0.0002	H-3→L+1 (59%), H-3→L+2 (28%)
26	325.5	0.0173	H-1→L+6 (33%), H-2→L+4 (29%), H-2→L+5 (17%), H-1→L+4 (7%)
27	323.4	0.0010	H-1→L+6 (40%), H-2→>L+4 (30%), H-1→L+5 (6%)
28	322.4	0.0006	H-3→L+4 (45%), H-3→L+5 (25%), H-1→L+6 (6%), H-3→L+3 (5%)
29	320.1	0.0006	H-4→L+4 (72%), H-2→L+3 (5%)
30	319.3	0.0004	H-8→L (46%), H-6→L (30%), H-5→L+1 (12%)
31	317.3	0.0415	H-5→L+1 (45%), H-5→L+2 (17%), H-2→L+3 (17%), H-8→L (10%)
32	317.0	0.0263	H-2→L+3 (62%), H-2→L+5 (6%), H-5→L+1 (6%)
33	312.5	0.0019	H-2→L+6 (30%), H-5→L+2 (26%), H-2→L+5 (17%), H-2→L+4 (6%)
34	312.1	0.0028	H→L+7 (73%), H-3→L+3 (9%)
35	311.4	0.0001	H-4→L+3 (30%), H-3→L+3 (29%), H→L+7 (13%), H-5→L+2 (8%), H-4→L+5 (6%)
36	311.2	0.0130	H-5→L+2 (31%), H-3→L+3 (17%), H-2→L+6 (15%), H-5→L+1 (12%)
37	310.4	0.0010	H-4→L+3 (38%), H-3→L+3 (27%), H-4→L+5 (8%)
38	308.0	0.0049	H-2→L+6 (28%), H-2→L+5 (24%), H-4→L+3 (10%), H-2→L+4 (6%)
39	307.8	0.0034	H-6→L+2 (34%), H-6→L+1 (19%)
40	306.8	0.0005	H-3→L+6 (52%), H-3→L+4 (14%), H-3→L+5 (11%)
41	306.0	0.0002	H-4→L+5(40%), H-4→L+3 (13%), H-4→L+8 (8%), H-2→L+6 (7%)
42	302.9	0.0004	H-3→L+5 (23%), H-3→L+4 (21%), H-3→L+6 (20%)
43	302.7	0.0005	H-7→L+1 (46%), H-10→L (33%)
44	301.3	0.0003	H-4→L+5 (13%), H-4→L+8 (13%), H-7→L+1 (11%), H-6→L+1 (7%), H-10→L (7%), H-5→L+4 (6%)
45	300.8	0.0074	H-1→L+7 (67%), H-2→L+7 (7%), H-5→L+4 (6%)
46	300.6	0.0002	H-4→L+5 (15%), H-3→L+5 (10%), H→L+15 (7%), H→L+8 (7%), H→L+11 (6%), H→L+12 (5%)
47	299.7	0.0057	H-5→L+4 (19%), H-8→L+1 (19%), H-1→L+7 (9%), H-6→L+2 (7%), H-6→L+1 (7%)
48	296.9	0.0005	H-10→L (28%), H-7→L+1 (26%), H-4→L+8 (11%)
49	296.3	0.0014	H-5→L+4 (39%), H-8→L+1 (11%), H-6→L+1 (11%), H→L+8 (9%), H-5→L+3 (6%)
50	295.7	0.0019	H→L+8 (63%)

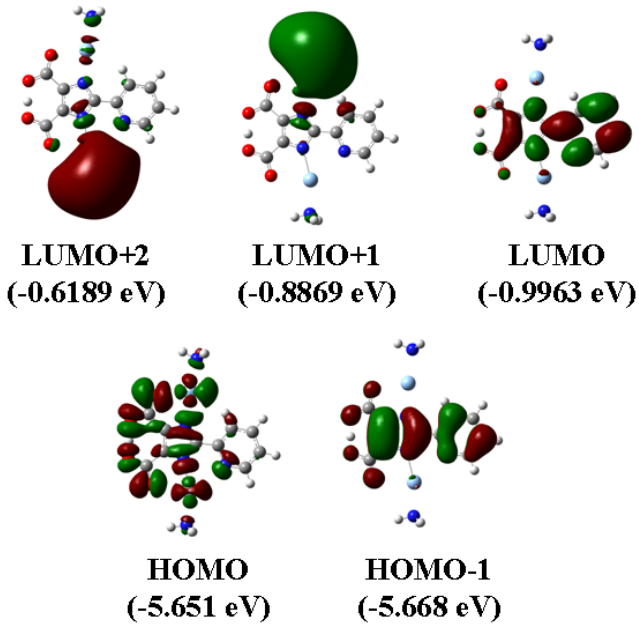

Fig. S21 Selected molecular orbitals for complex **1** (isovalue=0.02). Orbital energies are given in the parenthesis.

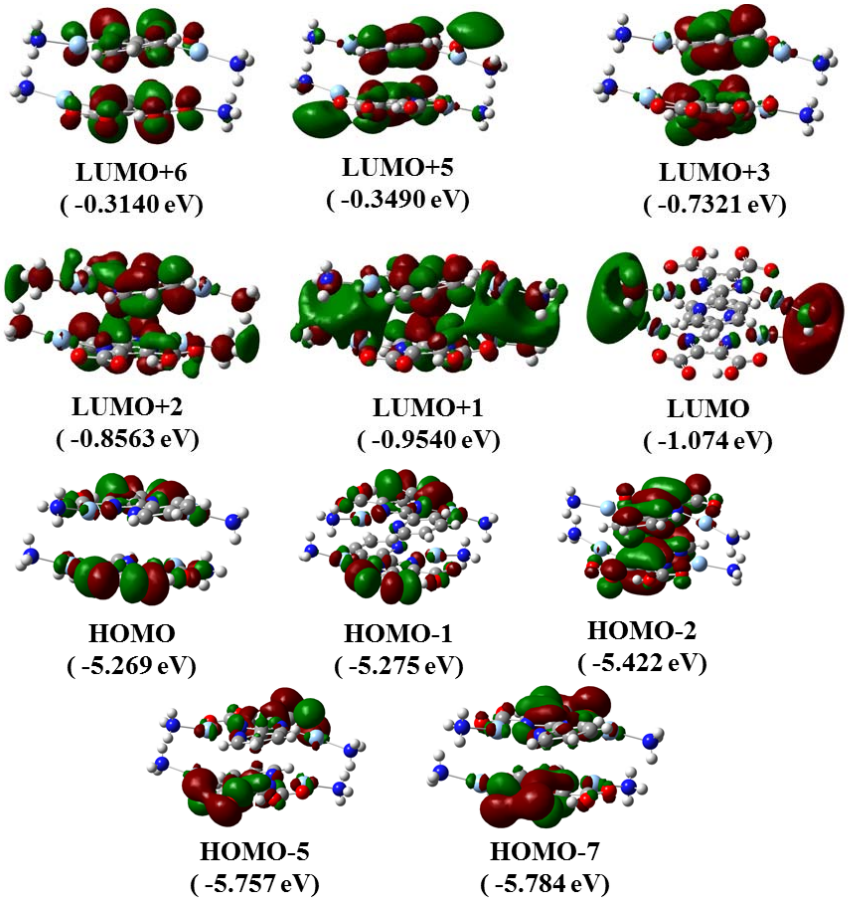

Fig. S22 Selected molecular orbitals for complex **2** (isovalue=0.02). Orbital energies are given in the parenthesis.

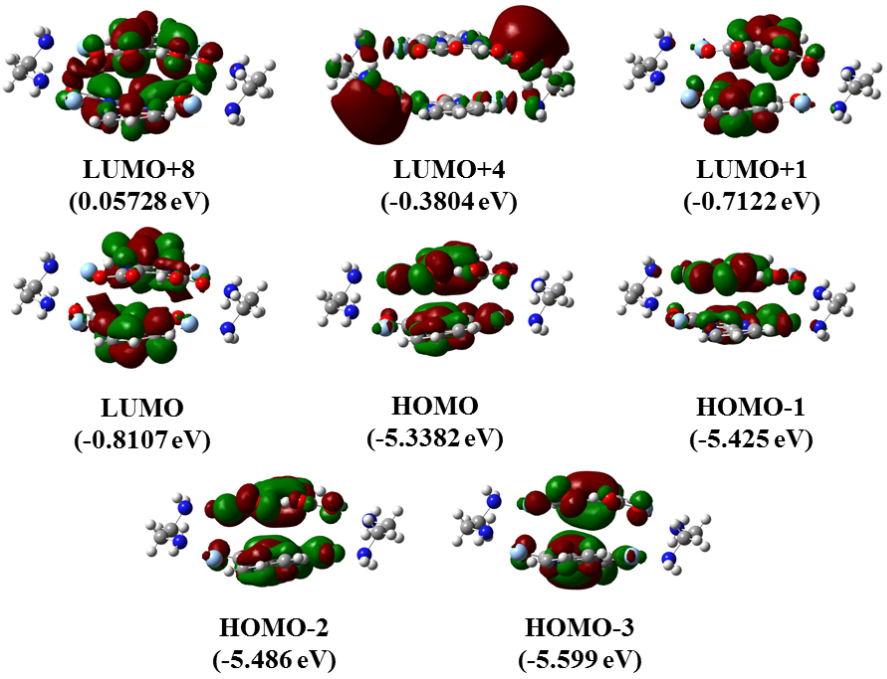

Fig. S23 Selected molecular orbitals for complex **3** (isovalue=0.02). Orbital energies are given in the parenthesis.

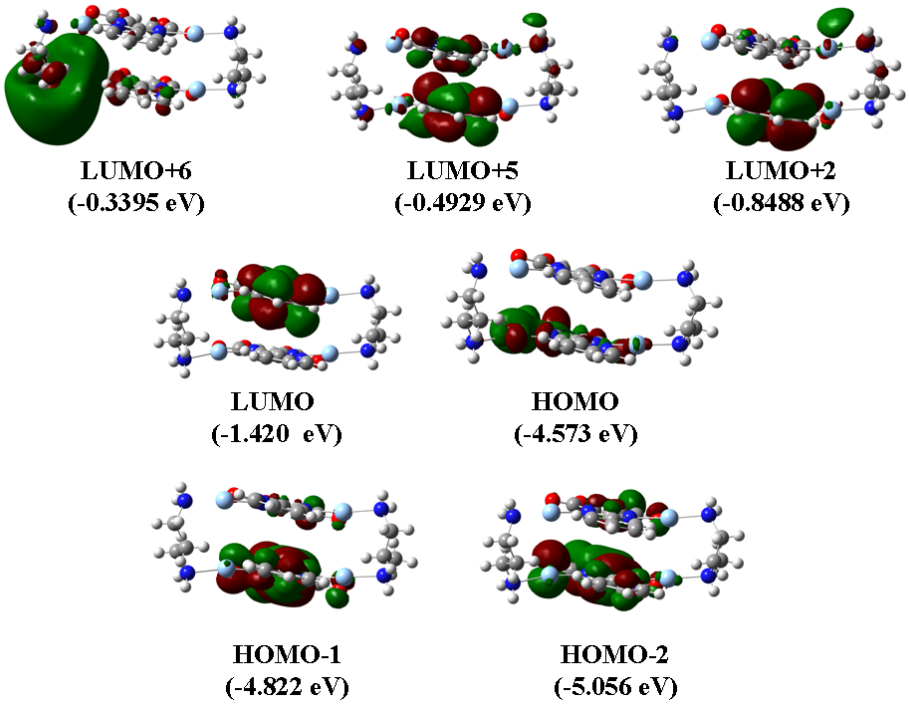

Fig. S24 Selected molecular orbitals for complex **4** (isovalue=0.02). Orbital energies are given in the parenthesis.

Table S12 Hirshfeld orbital compositions of selected molecular orbitals of **1.** The NAO compositions of HOMOs were given in parenthesis (H=HOMO, L=LUMO).

	H-1	H	L	L+1	L+2
Ag	0.93 (0.38)	26.30 (23.83)	4.84	39.71	42.22
NH_3	0.02 (0.00)	1.62 (1.57)	0.34	50.48	48.26
$Hpidc^{2-}$	99.05 (99.62)	72.08 (74.60)	94.83	9.81	9.52

Table S13 Hirshfeld orbital compositions of selected molecular orbitals of **2.** The NAO compositions of HOMOs were given in parenthesis (H=HOMO, L=LUMO).

	L	L+1	L+2	L+3	L+5	L+6
Ag	30.80	24.94	20.07	6.86	29.35	26.83
NH_3	61.33	28.21	26.25	2.65	16.50	25.55
$Hpidc^{2-}$	7.87	46.85	53.68	90.49	54.15	47.62
	H-7	H-5	H-2	H-1	H	
Ag	4.34 (3.33)	4.52 (3.66)	1.44 (0.82)	7.85 (6.27)	6.68 (5.07)	
NH_3	0.31 (0.22)	0.33 (0.23)	0.08 (0.06)	0.64 (0.52)	0.45 (0.35)	
$Hpidc^{2-}$	95.35 (96.45)	95.15 (96.11)	98.48 (99.11)	91.52 (93.21)	92.86 (94.58)	

Table S14 Hirshfeld orbital compositions of selected molecular orbitals of **3.** The NAO compositions of HOMOs were given in parenthesis (H=HOMO, L=LUMO).

	H-3	H-2	H-1	H	L	L+1	L+4	L+8
Ag	2.73 (1.96)	6.31 (4.91)	8.42 (6.87)	4.74 (3.50)	7.98	11.87	34.00	7.87
en	0.22 (0.14)	0.60 (0.53)	1.00 (0.87)	0.34 (0.26)	1.29	3.73	22.82	1.83
$Hpidc^{2-}$	97.05 (97.90)	93.10 (94.56)	90.58 (92.26)	94.92 (96.24)	90.73	84.40	43.18	90.31

Table S15 Hirshfeld orbital compositions of selected molecular orbitals of **4.** The NAO compositions of HOMOs were given in parenthesis (H=HOMO, L=LUMO).

	H-2	H-1	H	L	L+2	L+5	L+6
Ag	1.84 (1.11)	1.04 (0.55)	5.36 (4.16)	4.50	10.39	13.32	34.40
pn	0.08 (0.04)	0.05 (0.03)	0.52 (0.38)	1.11	8.91	11.64	51.37
$Hpidc^{2-}$	98.08 (98.85)	98.91 (99.42)	94.12 (95.46)	94.40	80.70	75.04	14.24

Table S16 Orbital energy (in eV) of HOMO, LUMO, and HOMO-LUMO gap for complex **1-4** (based on the calculation models in the simulation of UV-Vis spectra).

	E(HOMO)	E(LUMO)	HOMO-LUMO gap
1	-5.651	-0.9963	4.655
2	-5.269	-1.074	4.195
3	-5.338	-0.8107	4.527
4	-4.573	-1.420	3.153

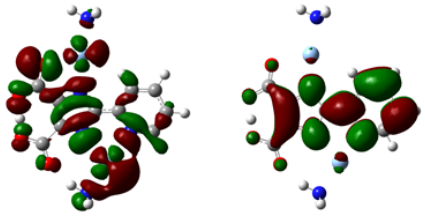

Fig. S25 Molecular orbital contours of higher singly occupied molecular orbital (HSOMO) and lower singly occupied molecular orbital (LSOMO) for the T_1 state of complex **1** (isovalue=0.02). Orbital energies are given in the parenthesis.

Table S17 The orbital energy levels for SOMOs of T_1 state for **1.**

	E(LSOMO)(eV)	E(HSOMO)(eV)	λ_{em} (nm)	The character of T_1 state
Ag	-6.096	-3.191	572.04	^{3}MLCT
NH_3				mixed
$Hpidc^{2-}$				^{3}ILCT

Table S18 Hirshfeld orbital compositions of frontier molecular orbitals for **1** based on differenr models. The NAO compositions of HOMOs were given in parenthesis (H=HOMO, L=LUMO, LS=LSOMO, HS=HSOMO).

	S_0 of Monomer of **1**		T_1 of Monomer of **1**		S_0 of Dimer of **1** (298 K)		S_0 of Dimer of **1** (100 K)		T_1 of Dimer of **1** (100 K)	
	H	L	LS	HS	H	L	H	L	LS	HS
Ag	26.30 (23.83)	4.84	37.81	4.10	8.22 (6.56)	35.04	8.68 (6.88)	34.37	23.04	14.91
NH3	1.62 (1.57)	0.34	3.96	0.23	0.63 (0.56)	58.56	0.68 (0.60)	59.37	2.01	7.33
Hpidc2-	72.08 (74.60)	94.83	58.23	95.68	91.15 (92.88)	6.40	90.64 (92.52)	6.26	74.95	77.77

Table S19 Hirshfeld orbital compositions of frontier molecular orbitals for **2** based on differenr models. The NAO compositions of HOMOs were given in parenthesis (H=HOMO, L=LUMO, LS=LSOMO, HS=HSOMO).

	S_0 of **2** (298 K)		T_1 of **2** (298 K)		S_0 of **2** (100 K)	
	H	L	LS	HS	H	L
Ag	6.68 (5.07)	30.80	11.03	6.57	7.07 (5.36)	29.84
NH3	0.45 (0.35)	61.33	0.90	0.91	0.49 (0.39)	61.20
Hpidc2-	92.86 (94.58)	7.87	88.06	92.52	92.44 (94.26)	8.97

Table S20 Hirshfeld orbital compositions of frontier molecular orbitals of S0 state for **3** and **4** based on differenr models. The NAO compositions of HOMOs were given in parenthesis (H=HOMO, L=LUMO).

	3				**4**			
	Tetranuclear Unit		Octanuclear Unit		Tetranuclear Unit		Octanuclear Unit	
	H	L	H	L	H	L	H	L
Ag	4.74 (3.50)	8.05	6.90 （5.36）	7.65	5.36 (4.16)	4.41	5.09 （3.96）	4.62
am	0.34 (0.26)	0.49	0.70 （0.59）	1.64	0.52 (0.38)	0.30	0.50 （0.37）	2.40
Hpidc2-	94.92 (96.24)	91.46	92.41 （94.05）	90.71	94.12 (95.46)	95.30	94.41 （95.68）	92.98

Table S21 Hirshfeld orbital compositions of frontier molecular orbitals of T1 state for **3** and **4** based on differenr models. The NAO compositions of HOMOs were given in parenthesis (LS=LSOMO, HS=HSOMO).

	3				**4**			
	Tetranuclear Unit		Octanuclear Unit		Tetranuclear Unit		Octanuclear Unit	
	LS	HS	LS	HS	LS	HS	LS	HS
Ag	12.29	7.49	0.94	1.24	0.61	0.87	5.02	4.99
am	0.99	1.02	90.10	91.95	93.17	94.45	0.52	1.93
Hpidc2-	86.72	91.49	8.96	6.81	6.21	4.69	94.46	93.08

References:

S1 (a) J. P. Perdew, K. Burke and M. Ernzerhof, *Phys. Rev. Lett.*, 1996, **77**, 3865; (b) J. P. Perdew, K. Burke and M. Ernzerhof, *Phys. Rev. Lett.*, 1997, **78**, 1396.

S2 (a) T. H. Dunning Jr., P. J. Hay, In Modern Theoretical Chemistry; Schaefer, H. F., III., Ed.; Plenum: New York, 1976; Vol. 3, 1-28; (b) P. J. Hay, W. R. Wadt, *J .Chem. Phys.,* 1985, **82**,

270; (c) W. R. Hadt, P. J. Hay, *J. Chem. Phys.*, 1985, **82**, 284; (d) P. J. Hay, W. R. Wadt, *J. Chem. Phys.*, 1985, **82**, 299.

S3 P. C. Hariharan and J. A. Pople, *Mol. Phys.,* 1974, **27**, 209.

S4 K. Burke and E. K. U. Gross, A guided tour of time-dependent density functional theory. In Density Functionals: Theory and Applications, Lecture Notes in Physics; D. Joubert, Ed.; Springer: New York, 1998; **500**.

S5 S. I. Gorelsky. SWizard Program; University of Ottawa: Ottawa, Canada, 2010; http://www.sg-chem.net/.

S6 S. I. Gorelsky and A. B. P. Lever, *J. Organomet. Chem.,* 2001, **635**, 187.

S7 F. L. Hirshfeld, *Theor. Chim. Acta (Berl.)* 1977, **44**, 129.

S8 T. Lu and F. W. Chen, *Acta Chim. Sin.* , 2011, **69**, 2393.

S9 (a) A. E. Reed and F.Weinhold, *J. Chem. Phys.,* 1983, **78**, 4066; (b) A. E. Reed, R. B. Weinstock and F. Weinhold, *J. Chem. Phys.,* 1985, **83**, 735.

S10 E. D. Glendering, A. E. Reed, J. E. Carpenter and F. Weinhold, NBO, version 3.1.

S11 I. Mayer, *Chem. Phys. Lett.* , 1983, **97**, 270.

S12 (a) T. Lu and F. W. Chen, *J. Comp. Chem.,* 2012, **33**, 580; (b) T. Lu, Multiwfn, Revison 2. 6. 1; University of Science and Technology Beijing: Beijing, China, 2013.

S13 M. J. Frisch, G. W. Trucks, H. B. Schlegel, G. E. Scuseria, M. A. Robb, J. R. Cheeseman, G. Scalmani, V. Barone, B. Mennucci, G. A. Petersson, H. Nakatsuji, M. Caricato, X. Li, H. P. Hratchian, A. F. Izmaylov, J. Bloino, G. Zheng, J. L. Sonnenberg, M. Hada, M. Ehara, K. Toyota, R. Fukuda, J. Hasegawa, M. Ishida, T. Nakajima, Y. Honda, O. Kitao, H. Nakai, T. Vreven, J. A. Montgomery, Jr., J. E. Peralta, F. Ogliaro, M. Bearpark, J. J. Heyd, E. Brothers, K. N. Kudin, V. N. Staroverov, R. Kobayashi, J. Normand, K. Raghavachari, A. Rendell, J. C. Burant, S. S. Iyengar, J. Tomasi, M. Cossi, N. Rega, J. M. Millam, M. Klene, J. E. Knox, J. B. Cross, V. Bakken, C. Adamo, J. Jaramillo, R. Gomperts, R. E. Stratmann, O. Yazyev, A. J. Austin, R. Cammi, C. Pomelli, J. Ochterski, R. L. Martin, K. Morokuma, V. G. Zakrzewski, G. A. Voth, P. Salvador, J. J. Dannenberg, S. Dapprich, A. D. Daniels, O. Farkas, J. B. Foresman, J. V. Ortiz, J. Cioslowski and D. J. Fox, GAUSSIAN 09 (Revision A.02), Gaussian, Inc., Wallingford, CT, 2009.